

Role of Interchain Hopping in the Magnetic Susceptibility of Quasi-One-Dimensional Electron Systems

Yuki FUSEYA^{1,2*}, Masahisa TSUCHIIZU¹, Yoshikazu SUZUMURA¹ and Claude BOURBONNAIS³

¹ *Department of Physics, Nagoya University, Nagoya 464-8602, Japan*

² *Department of Physics, University of Tokyo, Hongo, Bunkyo-ku, Tokyo 133-0033, Japan*

³ *Regroupement Québécois sur les Matériaux de Pointe, Département de physique, Université de Sherbrooke, Sherbrooke, Québec, Canada, J1K-2R1*

The role of interchain hopping in quasi-one-dimensional (Q-1D) electron systems is investigated by extending the Kadanoff-Wilson renormalization group of one-dimensional (1D) systems to Q-1D systems. This scheme is applied to the extended Hubbard model to calculate the temperature (T) dependence of the magnetic susceptibility, $\chi(T)$. The calculation is performed by taking into account not only the logarithmic Cooper and Peierls channels, but also the non-logarithmic Landau and finite momentum Cooper channels, which give relevant contributions to the uniform response at finite temperatures. It is shown that the interchain hopping, t_{\perp} , reduces $\chi(T)$ at low temperatures, while it enhances $\chi(T)$ at high temperatures. This notable t_{\perp} dependence is ascribed to the fact that t_{\perp} enhances the antiferromagnetic spin fluctuation at low temperatures, while it suppresses the 1D fluctuation at high temperatures. The result is at variance with the random-phase-approximation approach, which predicts an enhancement of $\chi(T)$ by t_{\perp} over the whole temperature range. The influence of both the long-range repulsion and the nesting deviations on $\chi(T)$ is further investigated. We discuss the present results in connection with the data of $\chi(T)$ in the (TMTTF)₂X and (TMTSF)₂X series of Q-1D organic conductors, and propose a theoretical prediction for the effect of pressure on magnetic susceptibility.

KEYWORDS: quasi-one dimension, magnetic susceptibility, renormalization group, extended-Hubbard model, long-range interaction, nesting deviation, crossover, (TMTTF)₂X, (TMTSF)₂X

1. Introduction

Interacting electrons in ordinary metals and semiconductors are usually described in the framework of the Landau's Fermi liquid (FL) theory.¹ What lies at the root of the Fermi liquid theory is the concept of single-particle excitations that behave as effective non-interacting electrons at low-energy. In one dimension, however, the FL picture is no longer valid due to the strongly enhanced correlation effects, which lead to the absence of quasi-particles and the emergence of decoupled collective spin and charge excitations, which characterize different quantum liquid phases such as the Tomonaga-Luttinger liquid (TLL).² While properties of the FL and TLL are independently well characterized, their relative importance for weakly coupled chains in the quasi-one-dimensional (Q-1D) case is much less understood. In Q-1D systems, a dimensional crossover between TLL and FL phases is expected to take place on the temperature scale. How such a crossover is achieved in practice is an important issue in weakly coupled chains of organic conductors (TMTCF)₂X ($C=S, Se, X=PF_6, Br, ClO_4, AsF_6, \text{etc.}$).

Such a crossover has been observed in transport properties of these materials.³ The temperature (T) dependence of resistivity (ρ) exhibits a power-law dependence $\rho \sim T^{\alpha}$ ($\alpha \sim 0.5$) for T above $T_x \sim 100\text{K}$, which is consistent with a TLL behavior.² It is followed by a T^2 dependence below T_x , which is expected in a FL. For the uniform magnetic susceptibility, χ , however, the expected temperature dependence below T_x is not known

theoretically. On experimental grounds, $\chi(T)$ does not show any change around T_x ,^{4,5} and is still temperature dependent. This indicates that the influence of the dimensional crossover may be quite specific to observable quantities. It is of particular interest to examine how the physical quantities of the Q-1D correlated electron systems are modified through T_x .

Some basic aspects of this dimensional crossover can be easily illustrated by first looking at the non-interacting case. When the interchain hopping t_{\perp} is much smaller than the intrachain one t , the Fermi surface consists of two slightly warped planes as shown in Fig. 1, where the energy scale of the warping is of order of t_{\perp} . Now when the temperature scale is much higher than t_{\perp} , the warping is incoherent due to thermal fluctuations, the quantum mechanical coherence of electrons is then thermally confined along the chains and the system is effectively one dimensional (1D). By contrast, for the energy scale much lower than t_{\perp} , the quantum coherence of electron extends over several chains, the warping of the Fermi surface becomes effective, and the system is considered as two- or three-dimensional. The scale t_{\perp} thus corresponds to the crossover temperature T_x for non-interacting electrons. The presence of interactions, however, modifies this picture by reducing the crossover scale, which leads $T_x^* \sim t(t_{\perp}/t)^{1/\phi}$ with $0 \leq \phi < 1$.⁶

The main theoretical difficulty in studying the Q-1D systems resides in the treatment of the 1D fluctuations which affect the coupling between chains and the restoration of a FL behavior. At the lowest order of 1D perturbation theory, non-FL behavior basically comes from

*E-mail address: fuseya@hosi.phys.s.u-tokyo.ac.jp

the quantum interference between the Cooper and the Peierls infrared instabilities. This is an effect that is not captured by approaches like random phase approximation (RPA), which are known to select only one type of instability. The bosonization approach and exact solutions based on the Bethe ansatz are extremely powerful in the purely 1D case, but are of limited use in higher dimension where FL quasi-particles become relevant excitations. The renormalization group (RG) technique for interacting electrons, however, can deal in a controlled way with both TLL and FL behaviors in weak coupling.

In this respect, on the basis of the Kadanoff-Wilson RG scheme, Duprat and Bourbonnais (DB) applied a *two-variable* momentum approximation for the coupling constants, from which the competition between density wave and superconducting states in Q-1D systems can be analyzed.⁷ By calculating the instability of the normal state towards an ordered state below the crossover scale T_x , they obtained the emergence of anisotropic superconductivity from spin-density-wave correlations due to the presence of nesting deviations. These effects were not treated in previous approaches, which are based on a sharp two cutoffs scaling procedure.⁸

At the end of the seventies, Lee *et al.* discussed the role of interchain (Coulomb) coupling using the RG technique but where t_\perp was excluded.⁹ In their work, not only density-wave and superconductive response functions were discussed, but also the uniform response, such as the compressibility and magnetic susceptibility. When the interchain hopping is present, however, further improvement of the RG method is needed to describe fluctuations that contribute to the uniform responses like magnetic susceptibility, compressibility and the Drude weight.

It is the purpose of the present study to further develop the Kadanoff-Wilson approach in the case of the Q-1D interacting electron systems to retain the *full transverse momentum-dependence* for the flow of coupling constants — a scheme that shall be denoted a N -chain RG in the following. We shall concentrate on the RG calculation of the uniform magnetic susceptibility and investigate the dimensional crossover behavior for this physical quantity that is directly relevant to experiment. The temperature dependence of the magnetic susceptibility $\chi(T)$ is calculated to show how $\chi(T)$ varies with the interchain hopping t_\perp , long-range interactions and nesting deviations which are well known to be relevant in organic conductors.

The paper is organized as follows. In §2, the model Hamiltonian is introduced with the formulation of the N -chain RG method. The RG flow trajectories for the couplings constants across the crossover region are given in §3. In §4, the $\chi(T)$ behavior in the Q-1D systems is calculated within two different approaches. We first consider the RPA method, which gives $\chi(T)$ to lowest order in t_\perp . The results are compared to the full N -chain RG treatment, where t_\perp is treated as non perturbatively. In §5, the results are discussed in connection with experimental data of (TMTCF)₂X compounds and we conclude in §6.

2. N-chain Renormalization Group

2.1 Model

We consider a linear array of N weakly coupled chains of length L at quarter filling, whose Hamiltonian $H = H_0 + H_I$ consists of a non interacting and interacting parts

$$H_0 = \sum_{i,j,\sigma} \left[-tc_{i,j,\sigma}^\dagger c_{i+1,j,\sigma} - t_\perp c_{i,j,\sigma}^\dagger c_{i,j+1,\sigma} + \text{h.c.} \right], \quad (1)$$

$$H_I = \sum_{i,j} [Un_{i,j,\uparrow}n_{i,j,\downarrow} + V_1n_{i,j}n_{i+1,j} + V_2n_{i,j}n_{i+2,j}]. \quad (2)$$

Here $c_{i,j,\sigma}$ ($c_{i,j,\sigma}^\dagger$) is an annihilation (a creation) operator of an electron on the i -th site of the j -th chain with spin σ ($=\uparrow, \downarrow$), and t (t_\perp) is the intrachain (interchain) hopping. The intrachain interaction part is of the extended Hubbard form with U as the onsite Coulomb repulsion, and V_1 (V_2) as the nearest- (next-nearest-) neighbor repulsion. The density operators are $n_{i,j,\sigma} = c_{i,j,\sigma}^\dagger c_{i,j,\sigma}$ and $n_{i,j} = n_{i,j,\uparrow} + n_{i,j,\downarrow}$. The kinetic term H_0 can be expressed in the weak-coupling region as follows:

$$H_0 = \sum_{p,\mathbf{k},\sigma} \xi_p(\mathbf{k}) c_{p,\mathbf{k},\sigma}^\dagger c_{p,\mathbf{k},\sigma}, \quad (3)$$

$$\xi_p(\mathbf{k}) \simeq v_F(pk - k_F) + \xi_\perp(k_\perp), \quad (4)$$

$$\xi_\perp(k_\perp) = -2t_\perp \cos k_\perp - 2t_{\perp 2} \cos 2k_\perp, \quad (5)$$

where v_F is the Fermi velocity and the lattice constants are set to be unity. The operator $c_{p,\mathbf{k},\sigma}$ ($c_{p,\mathbf{k},\sigma}^\dagger$) annihilates (creates) an electron with spin σ close to the Fermi surface of the right $k \simeq +k_F$ ($p = +1$) and left $k \simeq -k_F$ ($p = -1$) branches. The second-harmonic term in eq. (5), which denotes the nesting deviation, is given by $t_{\perp 2} = t_\perp^2 \cos k_F / 4t \sin^2 k_F$ within the tight-binding approximation, however, we consider t_\perp and $t_{\perp 2}$ as independent parameters in this paper in order to distinguish the problem of the dimensionality and the nesting deviations. As it will be shown later, $t_{\perp 2}$ does not affect the magnetic susceptibility.

The partition function $Z (= \text{Tr} e^{-\beta H})$ is written in the functional integral form

$$Z = \iint \mathcal{D}\psi^* \mathcal{D}\psi e^{S[\psi^*, \psi]}, \quad (6)$$

where the ψ 's are the Grassmann fields. The action S is given by

$$S[\psi^*, \psi] = S_0[\psi^*, \psi] + S_I[\psi^*, \psi], \quad (7)$$

$$S_0[\psi^*, \psi] = \sum_{p,\tilde{k},\sigma} [\mathfrak{G}_p^0(\tilde{k})]^{-1} \psi_{p,\sigma}^*(\tilde{k}) \psi_{p,\sigma}(\tilde{k}), \quad (8)$$

$$S_I[\psi^*, \psi] = -\frac{T}{LN} \sum_{p,\tilde{q}} [g_\rho \rho_p(\tilde{q}) \rho_{-p}(-\tilde{q}) + g_\sigma \mathbf{S}_p(\tilde{q}) \cdot \mathbf{S}_{-p}(-\tilde{q}) + g_{4\rho} \rho_p(\tilde{q}) \rho_p(-\tilde{q}) + g_{4\sigma} S_p^z(\tilde{q}) S_p^z(-\tilde{q})], \quad (9)$$

where \tilde{k} (\tilde{q}) indicates the vector in the Fourier-Matsubara space $\tilde{k} = (\mathbf{k}, \omega_n)$ ($\tilde{q} = (\mathbf{q}, \omega_m)$) with $\omega_n = (2n + 1)\pi T$

($\omega_m = 2m\pi T$). Here, the charge and spin-density operators of the branch p are given by

$$\rho_p(\tilde{q}) \equiv \frac{1}{2} \sum_{\tilde{k}, \sigma} \psi_{p,\sigma}^*(\tilde{k} + \tilde{q}) \psi_{p,\sigma}(\tilde{k}), \quad (10)$$

$$\mathbf{S}_p(\tilde{q}) \equiv \frac{1}{2} \sum_{\tilde{k}, \alpha, \beta} \psi_{p,\alpha}^*(\tilde{k} + \tilde{q}) \boldsymbol{\sigma}^{\alpha\beta} \psi_{p,\beta}(\tilde{k}), \quad (11)$$

where $\psi_{p,\sigma}(\tilde{k})$ is the Grassmann field corresponding to $c_{p,\mathbf{k},\sigma}$. The bare Green's function is given by $\mathfrak{G}_p^0(\tilde{k}) = [i\omega_n - \xi_p(\mathbf{k})]^{-1}$. The coupling constants at quarter filling ($k_F = \pi/4$, $v_F = \sqrt{2}t$) are expressed in terms of U , V_1 and V_2 as follows

$$g_\rho = U + 4V_1 + 6V_2, \quad (12)$$

$$g_\sigma = -U + 2V_2, \quad (13)$$

$$g_{4\rho} = U + 4V_1 + 4V_2, \quad (14)$$

$$g_{4\sigma} = -U. \quad (15)$$

2.2 Renormalization Group

In the present N -chain RG, we achieved improvements for the Kadanoff-Wilson RG method by DB.⁷ The main improvements are made on the following points.

(1) *The non-logarithmic channels*, which are the particle-hole (Landau) and the particle-particle (Cooper+) channel on the same branch, are taken into account. The non-logarithmic channels have been neglected in the previous RG, but become important at finite temperatures, since the logarithmic terms are suppressed by the temperature and become comparable to the non-logarithmic terms. These non-logarithmic terms contribute to the renormalization of $g_{4\rho,4\sigma}$, and are in turn involved in the calculation of magnetic susceptibility.

(2) *The couplings depends on full (three) momenta* ($k_{1\perp}, k_{2\perp}, k_{3\perp}$); the forth momentum $k_{4\perp}$ is determined uniquely by the momentum conservation. Here, \mathbf{k}_1 and \mathbf{k}_2 are the incoming momenta and \mathbf{k}_3 and $\mathbf{k}_4 = \mathbf{k}_1 + \mathbf{k}_2 - \mathbf{k}_3$ are the outgoing ones. When we consider the only fixed $\mathbf{k}_1 = \mathbf{k}_2$ for the Cooper channel and neglect the non-logarithmic channels, two variables \mathbf{k}_1 and \mathbf{k}_3 are enough to describe the momentum dependence of the couplings. This scheme has been employed by DB. However, when we consider all scattering channels, namely the Cooper, Peierls, Landau and Cooper+ channels, the couplings can be successfully described by three ($\mathbf{k}_1, \mathbf{k}_2, \mathbf{k}_3$) instead of two variables. In order to investigate the temperature dependence of the physical quantities, we calculate the RG at the finite temperature where the Landau channel plays an important role. So we keep three variables in the present N -chain RG technique despite the complicated formulation.

Based on the Kadanoff-Wilson RG procedure, we calculate the effective action $S[\psi^*, \psi]_\ell$ at the renormalized bandwidth $E_0(\ell)$. The partial integration is carried out for momentum located in the energy shell $E_0(\ell)d\ell$ on both sides of the Fermi level (Fig. 1), where $E_0(\ell) = E_0 e^{-\ell}$ is the renormalized bandwidth at step ℓ of integration with the initial bandwidth $E_0 = 2v_F k_F \simeq 2t$.

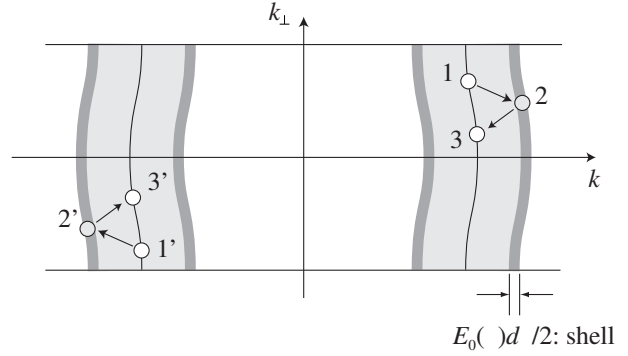


Fig. 1. Illustration of the partial integration. The initial states (1 & 1') are scattered to the excited states (2 & 2'), and then to the final state (3 & 3'). The contribution of the excited state located in the energy shell $E_0(\ell)d\ell/2$ are renormalized in the “new” renormalized action $S[\psi^*, \psi]_{\ell+d\ell}$.

By assuming the partition function invariant under the RG procedure, the renormalized action is obtained from

$$\begin{aligned} Z &= e^{A(\ell)} \iint \mathcal{D}\psi^* \mathcal{D}\psi e^{S[\psi^*, \psi]_\ell} \iint \mathcal{D}\bar{\psi}^* \mathcal{D}\bar{\psi} e^{S[\psi^*, \psi, \bar{\psi}^*, \bar{\psi}]_{\ell+d\ell}} \\ &= e^{A(\ell+d\ell)} \iint \mathcal{D}\psi^* \mathcal{D}\psi e^{S[\psi^*, \psi]_{\ell+d\ell}}, \end{aligned} \quad (16)$$

where $A(\ell)$ corresponds to the free energy density at the step ℓ . The partial integration with respect to $\bar{\psi}$ and $\bar{\psi}^*$ can be performed by making use of the linked cluster theorem. Then the renormalized action is expressed as

$$\begin{aligned} S[\psi^*, \psi]_{\ell+d\ell} &= S[\psi^*, \psi]_\ell \\ &+ \sum_{n=1}^{\infty} \frac{1}{n!} \left\langle \left(\sum_{i=1}^4 S_{1,i}[\psi^*, \psi, \bar{\psi}^*, \bar{\psi}] \right)^n \right\rangle, \end{aligned} \quad (17)$$

where $S_{1,i}$ has $i = 1 \sim 4$ $\bar{\psi}$'s in the outer shell, and

$$\langle \dots \rangle = \frac{\int \int \mathcal{D}\bar{\psi}^* \mathcal{D}\bar{\psi} (\dots) e^{S_0[\bar{\psi}^*, \bar{\psi}]}}{\int \int \mathcal{D}\bar{\psi}^* \mathcal{D}\bar{\psi} e^{S_0[\bar{\psi}^*, \bar{\psi}]}}. \quad (18)$$

The renormalizations of $g_{\rho,\sigma,4\rho,4\sigma}$ at the one-loop level ($n = 2$) are obtained from the outer-shell averages of the quadratic term of the action, i.e., $\frac{1}{2} \langle (S_{1,2})^2 \rangle$. Depending on the way of choosing two $\bar{\psi}$ among four, $S_{1,2}$ is decomposed into four components as

$$S_{1,2} = S_{1,2}^C + S_{1,2}^P + S_{1,2}^L + S_{1,2}^{C+}. \quad (19)$$

The corresponding diagrams are shown in Fig. 2. The definitions of $S_{1,2}^\mu$ are given below. Each $S_{1,2}^\mu$ is orthogonal, so that the contractions in each channel μ can be considered independently. Finally, the renormalized action is obtained as

$$S[\psi^*, \psi]_{\ell+d\ell} - S[\psi^*, \psi]_\ell = \frac{1}{2} \sum_{\mu} \langle (S_{1,2}^\mu)^2 \rangle, \quad (20)$$

where $\mu = C, P, L, C+$ are related to the Cooper, Peierls, Landau, and Cooper+ channels, respectively.

The renormalized action at the one-loop level is obtained from the shell averages of the quadratic term of

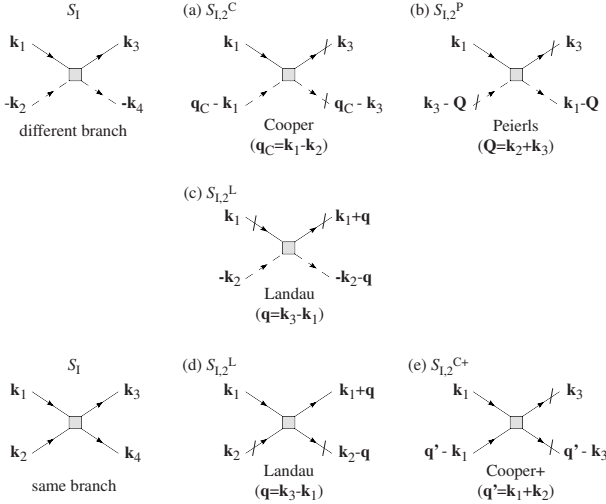


Fig. 2. Diagrams of $S_{I,2}$ for (a) Cooper, (b) Peierls, (c) Landau representations on the different branch, and (d) Landau, (e) Cooper+ representations on the same branch. The solid (dashed) line indicates right (left)-going electrons. The slashed lines refer to a Grassmann field in the outer shell, $\tilde{\psi}$.

the action $S_{I,2}$, which is given in eq. (19). The contraction is performed by the outer shell average of all pairs of two $\tilde{\psi}$'s. Each one is given by

$$S_{I,2}^C = -\frac{T}{LN} \sum_{\tilde{k}_{1,3}, \tilde{q}_C} \sum_P [g_{ss}(k_{1\perp}, k_{1\perp} - q_C, k_{3\perp}) \times \bar{\Delta}_{ss,p}^*(\tilde{q}_C, \tilde{k}_3) \Delta_{ss,p}(\tilde{q}_C, \tilde{k}_1) + g_{ts}(k_{1\perp}, k_{1\perp} - q_C, k_{3\perp}) \bar{\Delta}_{ts,p}^*(\tilde{q}_C, \tilde{k}_3) \Delta_{ts,p}(\tilde{q}_C, \tilde{k}_1) + \text{c.c.}], \quad (21)$$

$$S_{I,2}^P = -\frac{T}{LN} \sum_{\tilde{k}_{1,3}, \tilde{Q}} \sum_P [g_C(k_{1\perp}, Q_{\perp} - k_{3\perp}, k_{3\perp}) \times \bar{\mathcal{O}}_{c,p}^*(\tilde{Q}, \tilde{k}_3) \mathcal{O}_{c,p}(\tilde{Q}, \tilde{k}_1) + g_s(k_{1\perp}, Q_{\perp} - k_{3\perp}, k_{3\perp}) \bar{\mathcal{O}}_{s,p}^*(\tilde{Q}, \tilde{k}_3) \mathcal{O}_{s,p}(\tilde{Q}, \tilde{k}_1) + \text{c.c.}], \quad (22)$$

$$S_{I,2}^{L-} = -\frac{T}{LN} \sum_{\tilde{k}_{1,2}, \tilde{q}} \sum_P [g_{\rho}(k_{1\perp}, k_{2\perp}, q_{\perp} + k_{1\perp}) \times \bar{\mathcal{O}}_{\rho,p}^*(\tilde{q}, \tilde{k}_1) \mathcal{O}_{\rho,-p}(\tilde{q}, \tilde{k}_2) + g_{\sigma}(k_{1\perp}, k_{2\perp}, q_{\perp} + k_{1\perp}) \bar{\mathcal{O}}_{\sigma,p}^*(\tilde{q}, \tilde{k}_1) \mathcal{O}_{\sigma,-p}(\tilde{q}, \tilde{k}_2) + g_{4\rho}(k_{1\perp}, k_{2\perp}, q_{\perp} + k_{1\perp}) \bar{\mathcal{O}}_{\rho,p}^*(\tilde{q}, \tilde{k}_1) \mathcal{O}_{\rho,p}(\tilde{q}, \tilde{k}_2) + g_{4\sigma}(k_{1\perp}, k_{2\perp}, q_{\perp} + k_{1\perp}) \bar{\mathcal{O}}_{\sigma,p}^{z*}(\tilde{q}, \tilde{k}_1) \mathcal{O}_{\sigma,p}^z(\tilde{q}, \tilde{k}_2) + \text{c.c.}], \quad (23)$$

$$S_{I,2}^{C+} = -\frac{T}{LN} \sum_{\tilde{k}_{1,3}, \tilde{q}'} \sum_P [g_{4||}(k_{1\perp}, q'_{\perp} - k_{1\perp}, k_{3\perp}) \times \bar{\Delta}_{4||,p}^*(\tilde{q}', \tilde{k}_3) \Delta_{4||,p}(\tilde{q}', \tilde{k}_1)$$

$$+ g_{4\perp}(k_{1\perp}, q'_{\perp} - k_{1\perp}, k_{3\perp}) \bar{\Delta}_{4\perp,p}^*(\tilde{q}', \tilde{k}_3) \Delta_{4\perp,p}(\tilde{q}', \tilde{k}_1) + \text{c.c.}], \quad (24)$$

where

$$\Delta_{ss,p}(\tilde{q}_C, \tilde{k}) \equiv \sum_{\alpha,\beta} (i\sigma_y) \psi_{-p,\alpha}(-\tilde{k} + \tilde{q}_C) \psi_{p,\beta}(\tilde{k}), \quad (25)$$

$$\Delta_{ts,p}(\tilde{q}_C, \tilde{k}) \equiv \sum_{\alpha,\beta} (i\sigma_x) \psi_{-p,\beta}(-\tilde{k} + \tilde{q}_C) \psi_{p,\alpha}(\tilde{k}), \quad (26)$$

$$\mathcal{O}_{c,p}(\tilde{Q}, \tilde{k}) \equiv \sum_{\sigma} \psi_{-p,\sigma}^*(\tilde{k} + \tilde{Q}) \psi_{p,\sigma}(\tilde{k}), \quad (27)$$

$$\mathcal{O}_{s,p}(\tilde{Q}, \tilde{k}) \equiv \sum_{\alpha,\beta} \psi_{-p,\alpha}^*(\tilde{k} + \tilde{Q}) \sigma^{\alpha\beta} \psi_{p,\beta}(\tilde{k}), \quad (28)$$

$$\mathcal{O}_{\rho,p}(\tilde{q}, \tilde{k}) \equiv \frac{1}{2} \sum_{\sigma} \psi_{p,\sigma}^*(\tilde{k} + \tilde{q}) \psi_{p,\sigma}(\tilde{k}), \quad (29)$$

$$\mathcal{O}_{\sigma,p}(\tilde{q}, \tilde{k}) \equiv \frac{1}{2} \sum_{\alpha,\beta} \psi_{p,\alpha}^*(\tilde{k} + \tilde{q}) \sigma^{\alpha\beta} \psi_{p,\beta}(\tilde{k}), \quad (30)$$

$$\Delta_{4||,p}(\tilde{q}', \tilde{k}) \equiv \frac{1}{2} \sum_{\sigma} \tau^{\sigma\sigma} \psi_{p,\sigma}(\tilde{q}' - \tilde{k}) \psi_{p,\sigma}(\tilde{k}), \quad (31)$$

$$\Delta_{4\perp,p}(\tilde{q}', \tilde{k}) \equiv \frac{1}{2} \sum_{\sigma} \tau^{\sigma\sigma} \psi_{p,-\sigma}^*(\tilde{q}' - \tilde{k}) \psi_{p,\sigma}(\tilde{q}'). \quad (32)$$

Here $\mathbf{q}_C \equiv \mathbf{k}_1 - \mathbf{k}_2$, $\mathbf{Q} \equiv \mathbf{k}_2 + \mathbf{k}_3$, $\mathbf{q} \equiv \mathbf{k}_3 - \mathbf{k}_1$ and $\mathbf{q}' \equiv \mathbf{k}_1 + \mathbf{k}_2$.

In terms of eqs. (12)-(15), the above coupling constants are written as

$$\begin{pmatrix} g_{ss}(k_{1,2,3\perp}) \\ g_{ts}(k_{1,2,3\perp}) \end{pmatrix} = \frac{1}{4} \begin{pmatrix} 1 & -3 \\ 1 & 1 \end{pmatrix} \begin{pmatrix} g_{\rho}(k_{1,2,3\perp}) \\ g_{\sigma}(k_{1,2,3\perp}) \end{pmatrix} \quad (33)$$

$$\begin{pmatrix} g_C(k_{1,2,3\perp}) \\ g_S(k_{1,2,3\perp}) \end{pmatrix} = \frac{1}{4} \begin{pmatrix} -1 & -3 \\ -1 & 1 \end{pmatrix} \begin{pmatrix} g_{\rho}(k_{1,2,3\perp}) \\ g_{\sigma}(k_{1,2,3\perp}) \end{pmatrix} \quad (34)$$

$$\begin{pmatrix} g_{4||}(k_{1,2,3\perp}) \\ g_{4\perp}(k_{1,2,3\perp}) \end{pmatrix} = \frac{1}{2} \begin{pmatrix} 1 & 1 \\ 1 & -1 \end{pmatrix} \begin{pmatrix} g_{4\rho}(k_{1,2,3\perp}) \\ g_{4\sigma}(k_{1,2,3\perp}) \end{pmatrix} \quad (35)$$

2.2.1 Cooper channel

The contraction of the Cooper channel at the one-loop level is carried out as

$$\frac{1}{2} \langle (S_{I,2}^C)^2 \rangle = \frac{T}{LN} \sum_{\nu=ss,ts} \sum_{\{\tilde{k}_{1,3}, \tilde{q}_C\}^*} \frac{d\ell}{N\nu v_F} \sum_{k'_{\perp}} I_C(q_C, q_{C\perp}, k'_{\perp}; \ell) \times g_{\nu}(k_{1\perp}, k_{1\perp} - q_{C\perp}, k'_{\perp}; \ell) g_{\nu}(k'_{\perp}, k'_{\perp} - q_{C\perp}, k_{3\perp}; \ell) \times \Delta_{\nu}^*(\tilde{q}_C, \tilde{k}_{3\perp}) \Delta_{\nu}(\tilde{q}_C, \tilde{k}_{1\perp}), \quad (36)$$

where

$$I_C(q_C, q_{C\perp}, k'_{\perp}; \ell) \equiv \frac{E_0(\ell)}{4} \sum_{\lambda=\pm 1} \frac{1}{E_0(\ell) + \lambda A_C(q_C, q_{C\perp}, k'_{\perp})} \times \left\{ \tanh \frac{E_0(\ell)}{4T} + \tanh \frac{E_0(\ell)/2 + \lambda A_C(q_C, q_{C\perp}, k'_{\perp})}{2T} \right\}, \quad (37)$$

$$A_C(q_C, q_{C\perp}, k'_{\perp}) \equiv v_F q_C + \xi_{\perp}(k'_{\perp}) - \xi_{\perp}(q_{C\perp} - k'_{\perp}), \quad (38)$$

$$v_F q_C \equiv \xi_{\perp}(k_{1\perp} - q_{C\perp}) - \xi_{\perp}(k_{1\perp}). \quad (39)$$

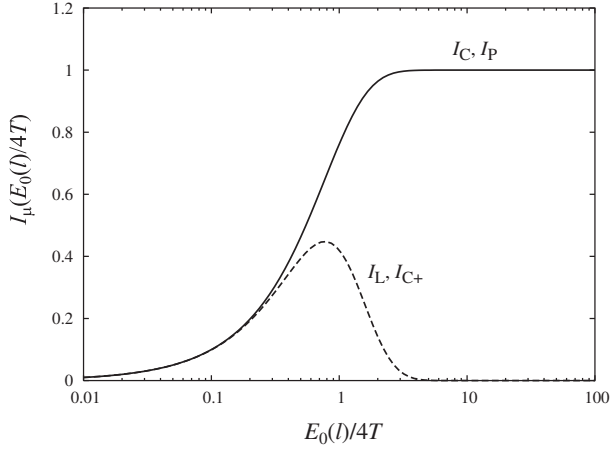


Fig. 3. Plots of $I_C(\mathbf{q}_C = 0)$, $I_P(\mathbf{Q} = \mathbf{Q}_0)$ (solid line), and $I_L(\mathbf{q} = 0)$, $I_{C+}(\mathbf{q}' = \mathbf{q}'_0)$ (dashed line) as a function of $E_0(\ell)/4T$, where $\mathbf{Q}_0 = (2k_F, \pi)$ and $\mathbf{q}'_0 = (2k_F, \pi)$. When the μ channel exhibits complete logarithmic divergence, I_μ reaches unity.

The function I_C indicates the degrees of logarithmic divergence; the case $I_C = 1$ implies a Cooper instability showing a complete logarithmic divergence, while it is partially suppressed for $I_C < 1$ (Fig. 3). This Cooper channel is shown diagrammatically in Fig. 4(a). We note that \mathbf{q}_C is set to be zero in DB's approach assuming that the Cooper instability is always logarithmic.

2.2.2 Peierls channel

At the one-loop level [Fig. 4(b)], the contraction in the Peierls channel is given by

$$\begin{aligned} & \frac{1}{2} \langle (S_{I,2}^P)^2 \rangle \\ &= \frac{T}{LN} \sum_{\nu=c,s} \sum_{\{\tilde{k}_{1,3}, \tilde{Q}\}^*} \frac{d\ell}{N\pi v_F} \sum_{k'_\perp} I_P(Q, Q_\perp, k'_\perp; \ell) \\ & \times g_\nu(k_{1\perp}, Q_\perp - k'_\perp, k'_\perp; \ell) g_\nu(k'_\perp, Q_\perp - k_{3\perp}, k_{3\perp}; \ell) \\ & \times \mathcal{O}_\nu^*(\tilde{Q}, \tilde{k}_{3\perp}) \mathcal{O}_\nu(\tilde{Q}, \tilde{k}_{1\perp}), \end{aligned} \quad (40)$$

where

$$\begin{aligned} I_P(Q, Q_\perp, k'_\perp; \ell) &\equiv \frac{E_0(\ell)}{4} \sum_{\lambda=\pm 1} \frac{1}{E_0(\ell) + \lambda A_P(Q, Q_\perp, k'_\perp)} \\ & \times \left\{ \tanh \frac{E_0(\ell)}{4T} + \tanh \frac{E_0(\ell)/2 + \lambda A_P(Q, Q_\perp, k'_\perp)}{2T} \right\}, \end{aligned} \quad (41)$$

$$A_P(Q, Q_\perp, k'_\perp) = v_F Q + \xi_\perp(k'_\perp) + \xi_\perp(k'_\perp - Q_\perp), \quad (42)$$

$$v_F Q = -\xi_\perp(k_{3\perp}) - \xi_\perp(Q_\perp - k_{3\perp}). \quad (43)$$

The flow of I_P is similar to I_C (Fig. 3).

2.2.3 Landau channel

The one-loop contraction of the Landau channel gives a non-logarithmic contribution to the RG equations. This channel was discarded in the previous RG. On the temperature scale, however, the non-logarithmic terms become effective when the Cooper and Peierls logarithmic singularities are suppressed. Moreover, the spin- and

charge-coupling terms (e.g., $g_\rho g_{4\sigma}$, $g_{4\rho} g_{4\sigma}$) give contributions of the same order of the spin- and charge-decoupling terms (e.g., g_ρ^2 , $g_\sigma g_{4\sigma}$)

The Landau contraction [Fig. 4(c)] yields (see Appendix A for the details)

$$\begin{aligned} & \frac{1}{2} \langle (S_{I,2}^L)^2 \rangle \\ &= \frac{T}{LN} \sum_{\nu, \nu'} \sum_{\{\tilde{k}_{1,2}, \tilde{q}\}^*} \frac{d\ell}{N\pi v_F} \sum_{k'_\perp} I_L(q, q_\perp, k'_\perp; \ell) \\ & \times g_\nu(k_{1\perp}, k'_\perp - q_\perp, k_{1\perp} + q_\perp; \ell) g_{\nu'}(k'_\perp, k_{2\perp}, k'_\perp - q_\perp; \ell) \\ & \times \mathcal{O}_\nu^*(\tilde{q}, \tilde{k}_{1\perp}) \mathcal{O}_{\nu'}(\tilde{q}, \tilde{k}_{2\perp}), \end{aligned} \quad (44)$$

where

$$\begin{aligned} I_L(q, q_\perp, k'_\perp; \ell) &\equiv \frac{E_0(\ell)}{4} \frac{1}{A_L(q, q_\perp, k'_\perp)} \\ & \times \left[\sum_{\lambda=\pm 1} \lambda \tanh \frac{E_0(\ell)/2 + \lambda A_L(q, q_\perp, k'_\perp)}{2T} \right], \end{aligned} \quad (45)$$

$$A_L(q, q_\perp, k'_\perp) = v_F q + \xi_\perp(k'_\perp) - \xi_\perp(k'_\perp - q_\perp), \quad (46)$$

$$v_F q = \xi_\perp(k_{1\perp}) - \xi_\perp(k_{1\perp} + q_\perp). \quad (47)$$

The function I_L does not reach the unity, i.e., the Landau channel is always non logarithmic (Fig. 3).

Similarly, the contraction of the Cooper+ channel at the one-loop level [Fig. 4(d)] is

$$\begin{aligned} & \frac{1}{2} \langle (S_{I,2}^{C+})^2 \rangle \\ &= \frac{T}{LN} \sum_{\nu, \nu'=4||, 4\perp} \sum_{\{\tilde{k}_{1,3}, \tilde{q}'\}^*} \frac{d\ell}{N\pi v_F} \sum_{k'_\perp} I_{C+}(q', q'_\perp, k'_\perp; \ell) \\ & \times g_\nu(k_{1\perp}, q'_\perp - k_{1\perp}, k'_\perp; \ell) g_{\nu'}(k'_\perp, q'_\perp - k'_\perp, k_{3\perp}; \ell) \\ & \times \Delta_\nu^*(\tilde{q}', \tilde{k}_{3\perp}) \Delta_{\nu'}(\tilde{q}', \tilde{k}_{1\perp}), \end{aligned} \quad (48)$$

where

$$\begin{aligned} I_{C+}(q', q'_\perp, k'_\perp; \ell) &\equiv \frac{E_0(\ell)}{4} \frac{1}{A_{C+}(q', q'_\perp, k'_\perp)} \\ & \times \left[\sum_{\lambda=\pm 1} \lambda \tanh \frac{E_0(\ell)/2 + \lambda A_{C+}(q', q'_\perp, k'_\perp)}{2T} \right], \end{aligned} \quad (49)$$

$$A_{C+}(q', q'_\perp, k'_\perp) = v_F q' + \xi_\perp(k'_\perp) + \xi_\perp(k'_\perp - q'_\perp), \quad (50)$$

$$v_F q' = -\xi_\perp(k_{1\perp}) - \xi_\perp(q'_\perp - k_{1\perp}). \quad (51)$$

2.2.4 Flow equations

Taking into account all the above one-loop contractions (Fig. 4), we can finally write the flow equations in the form

$$\frac{d}{d\ell} G_\nu(k_{1\perp}, k_{2\perp}, k_{3\perp}) = \frac{1}{N} \sum_{k'_\perp} F_\nu(k_{1\perp}, k_{2\perp}, k_{3\perp}, k'_\perp). \quad (52)$$

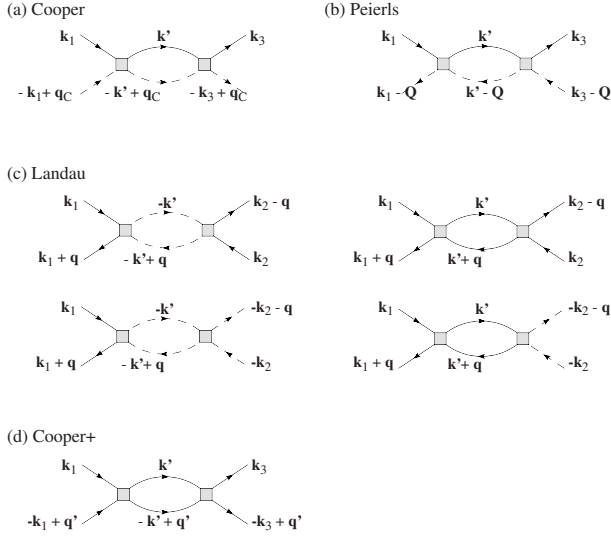


Fig. 4. Diagrams considered in the flow equations at the one-loop level. Here, $\mathbf{q}_C = \mathbf{k}_1 - \mathbf{k}_2$, $\mathbf{Q} = \mathbf{k}_2 + \mathbf{k}_3$, $\mathbf{q} = \mathbf{k}_3 - \mathbf{k}_1$ and $\mathbf{q}' = \mathbf{k}_1 + \mathbf{k}_2$

Here, ν denotes the type of the coupling, $\nu = \rho, \sigma, 4\rho, 4\sigma$. The function F_ν contains the quadratic terms of the coupling $G_\nu (= g_\nu/\pi v_F)$ and the contributions of the loop I_μ . The F_ν 's are given by

$$\begin{aligned}
F_\rho(k_{1\perp}, k_{2\perp}, k_{3\perp}, k'_\perp) &= -\frac{1}{4}I_C(q_C, q_{C\perp}, k'_\perp) \\
&\times [G_\rho(k_{1\perp}, k_{1\perp} - q_{C\perp}, k'_\perp)G_\rho(k'_\perp, k'_\perp - q_{C\perp}, k_{3\perp}) \\
&+ 3G_\sigma(k_{1\perp}, k_{1\perp} - q_{C\perp}, k'_\perp)G_\sigma(k'_\perp, k'_\perp - q_{C\perp}, k_{3\perp})] \\
&+ \frac{1}{4}I_P(Q, Q_\perp, k'_\perp) \\
&\times [G_\rho(k_{1\perp}, Q_\perp - k'_\perp, k'_\perp)G_\rho(k'_\perp, Q_\perp - k_{3\perp}, k_{3\perp}) \\
&+ 3G_\sigma(k_{1\perp}, Q_\perp - k'_\perp, k'_\perp)G_\sigma(k'_\perp, Q_\perp - k_{3\perp}, k_{3\perp})] \\
&+ \frac{1}{8}I_L(q, q_\perp, k'_\perp) \\
&\times [-G_\rho(k_{1\perp}, k'_\perp - q_\perp, q_\perp + k_{1\perp})G_{4\rho}(k'_\perp, k_{2\perp}, k'_\perp - q_\perp) \\
&- G_{4\rho}(k_{1\perp}, k'_\perp - q_\perp, q_\perp + k_{1\perp})G_\rho(k'_\perp, k_{2\perp}, k'_\perp + q_\perp; \ell) \\
&+ G_\rho(k_{1\perp}, k'_\perp - q_\perp, q_\perp + k_{1\perp})G_{4\sigma}(k'_\perp, k_{2\perp}, k'_\perp - q_\perp) \\
&+ G_{4\sigma}(k_{1\perp}, k'_\perp - q_\perp, q_\perp + k_{1\perp})G_\rho(k'_\perp, k_{2\perp}, k'_\perp + q_\perp)], \quad (53)
\end{aligned}$$

$$\begin{aligned}
F_\sigma(k_{1\perp}, k_{2\perp}, k_{3\perp}, k'_\perp) &= \frac{1}{4}I_C(q_C, q_{C\perp}, k'_\perp) \\
&\times [2G_\sigma(k_{1\perp}, k_{1\perp} - q_{C\perp}, k'_\perp)G_\sigma(k'_\perp, k'_\perp - q_{C\perp}, k_{3\perp}) \\
&- G_\rho(k_{1\perp}, k_{1\perp} - q_{C\perp}, k'_\perp)G_\sigma(k'_\perp, k'_\perp - q_{C\perp}, k_{3\perp}) \\
&- G_\sigma(k_{1\perp}, k_{1\perp} - q_{C\perp}, k'_\perp)G_\rho(k'_\perp, k'_\perp - q_{C\perp}, k_{3\perp})] \\
&+ \frac{1}{4}I_P(Q, Q_\perp, k'_\perp) \\
&\times [2G_\sigma(k_{1\perp}, Q_\perp - k'_\perp, k'_\perp)G_\sigma(k'_\perp, Q_\perp - k_{3\perp}, k_{3\perp}) \\
&+ G_\rho(k_{1\perp}, Q_\perp - k'_\perp, k'_\perp)G_\sigma(k'_\perp, Q_\perp - k_{3\perp}, k_{3\perp}) \\
&+ G_\sigma(k_{1\perp}, Q_\perp - k'_\perp, k'_\perp)G_\rho(k'_\perp, Q_\perp - k_{3\perp}, k_{3\perp})]
\end{aligned}$$

$$\begin{aligned}
&+ \frac{1}{8}I_L(q, q_\perp, k'_\perp) \\
&\times [G_\sigma(k_{1\perp}, k'_\perp - q_\perp, q_\perp + k_{1\perp})G_{4\rho}(k'_\perp, k_{2\perp}, k'_\perp - q_\perp) \\
&+ G_{4\rho}(k_{1\perp}, k'_\perp - q_\perp, q_\perp + k_{1\perp})G_\sigma(k'_\perp, k_{2\perp}, k'_\perp + q_\perp; \ell) \\
&- G_\sigma(k_{1\perp}, k'_\perp - q_\perp, q_\perp + k_{1\perp})G_{4\sigma}(k'_\perp, k_{2\perp}, k'_\perp - q_\perp) \\
&- G_{4\sigma}(k_{1\perp}, k'_\perp - q_\perp, q_\perp + k_{1\perp})G_\sigma(k'_\perp, k_{2\perp}, k'_\perp + q_\perp)], \quad (54)
\end{aligned}$$

$$\begin{aligned}
F_{4\rho}(k_{1\perp}, k_{2\perp}, k_{3\perp}, k'_\perp) &= \frac{1}{4}I_L(q, q_\perp, k'_\perp) \\
&\times [-2G_\rho(k_{1\perp}, k'_\perp - q_\perp, q_\perp + k_{1\perp})G_\rho(k'_\perp, k_{2\perp}, k'_\perp - q_\perp) \\
&+ G_{4\rho}(k_{1\perp}, k'_\perp - q_\perp, q_\perp + k_{1\perp})G_{4\rho}(k'_\perp, k_{2\perp}, k'_\perp + q_\perp; \ell) \\
&+ G_{4\sigma}(k_{1\perp}, k'_\perp - q_\perp, q_\perp + k_{1\perp})G_{4\sigma}(k'_\perp, k_{2\perp}, k'_\perp - q_\perp) \\
&+ G_{4\rho}(k_{1\perp}, k'_\perp - q_\perp, q_\perp + k_{1\perp})G_{4\sigma}(k'_\perp, k_{2\perp}, k'_\perp + q_\perp) \\
&+ G_{4\sigma}(k_{1\perp}, k'_\perp - q_\perp, q_\perp + k_{1\perp})G_{4\rho}(k'_\perp, k_{2\perp}, k'_\perp + q_\perp)] \\
&- \frac{1}{4}I_{C+}(q', q'_\perp, k'_\perp) \\
&\times [G_{4\rho}(k_{1\perp}, q'_\perp - k'_{1\perp}, k'_\perp)G_{4\rho}(k'_\perp, q'_\perp - k'_\perp, k_{3\perp}) \\
&+ G_{4\sigma}(k_{1\perp}, q'_\perp - k'_{1\perp}, k'_\perp)G_{4\sigma}(k'_\perp, q'_\perp - k'_\perp, k_{3\perp})], \quad (55)
\end{aligned}$$

$$\begin{aligned}
F_{4\sigma}(k_{1\perp}, k_{2\perp}, k_{3\perp}, k'_\perp) &= \frac{1}{2}I_L(q, q_\perp, k'_\perp) \\
&\times [-3G_\sigma(k_{1\perp}, k'_\perp - q_\perp, q_\perp + k_{1\perp})G_\sigma(k'_\perp, k_{2\perp}, k'_\perp - q_\perp) \\
&+ G_{4\rho}(k_{1\perp}, k'_\perp - q_\perp, q_\perp + k_{1\perp})G_{4\sigma}(k'_\perp, k_{2\perp}, k'_\perp + q_\perp) \\
&+ G_{4\sigma}(k_{1\perp}, k'_\perp - q_\perp, q_\perp + k_{1\perp})G_{4\rho}(k'_\perp, k_{2\perp}, k'_\perp + q_\perp)] \\
&- \frac{1}{4}I_{C+}(q', q'_\perp, k'_\perp) \\
&\times [G_{4\rho}(k_{1\perp}, q'_\perp - k'_{1\perp}, k'_\perp)G_{4\sigma}(k'_\perp, q'_\perp - k'_\perp, k_{3\perp}) \\
&+ G_{4\sigma}(k_{1\perp}, q'_\perp - k'_{1\perp}, k'_\perp)G_{4\rho}(k'_\perp, q'_\perp - k'_\perp, k_{3\perp})], \quad (56)
\end{aligned}$$

If we neglect the k_\perp -dependence, these flow equations agree with those obtained in the 1D limit [eqs. (11)-(15) in Ref. 10]. Calculating simultaneously these differential equations, we can obtain the renormalized couplings at each temperature. For the calculation of the N -chain system problem ($2N$ points on the Fermi surface), we solve $4N^3$ differential equations.

3. Flow of couplings & crossover behavior

In this section, we show the results of the numerical solutions of the flow equations (52) ~ (56) for $N = 31$ -chain systems with $U = 3t$, $V_1 = V_2 = 0$, $t_\perp = 0.01t$ at $T = 10^{-4}t$, and analyze the flow of the couplings. We set the minimum of the renormalized bandwidth, $E_0(\ell_c)$, of the order of $10^{-8}E_0$, which is low enough for $T = 10^{-4} \sim 10^{-6}t$. For $N \gtrsim 9$, the results become essentially independent of the number of chains. The present N -chain RG exhibits a clear difference in the property of spin gap between the odd-number chains (gapless) and the even-number chains (gapped). The aim of the present paper is to investigate the many-chain systems, where

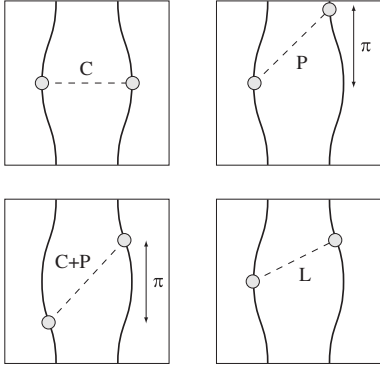
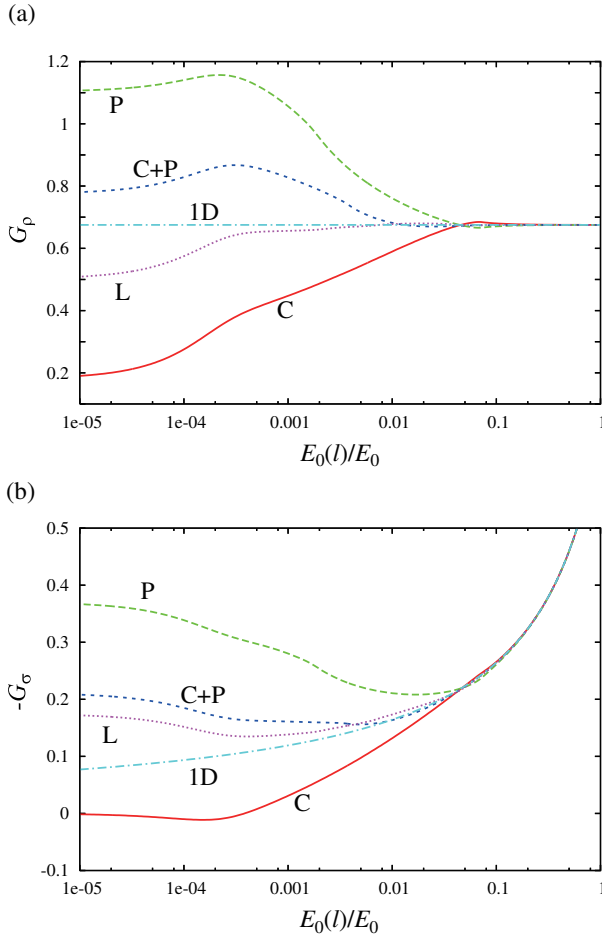


Fig. 5. Illustrations of the coupling C, P, C+P, L.

Fig. 6. (Color online) Energy flow of the couplings G_ρ (a) and $-G_\sigma$ (b) for $U = 3.0t, V_1 = V_2 = 0, t_\perp = 0.01t$ at $T = 10^{-4}t$.

the spin-gap does not open, so that we focus on the odd-number-chain systems in the present paper.

The renormalized couplings G_ν depends on three variables ($k_{1\perp}, k_{2\perp}, k_{3\perp}$). In order to see the essential points of the renormalized couplings, we show the energy flow of the couplings for some typical pairs:

(C) $G_\nu(0, 0, 0)$: the scattering of the Cooper pair $k_{1\perp} = k_{2\perp} = 0$.

(P) $G_\nu(\pi, 0, \pi)$: the scattering of the Peierls pair $k_{1\perp} \simeq \pi$ and $-k_{2\perp} \simeq 0$.

(C+P) $G_\nu(\pi/2, \pi/2, \pi/2)$: the scattering of the pair $k_{1\perp} \simeq \pi/2$ and $-k_{2\perp} \simeq -\pi/2$, where the Cooper and Peierls instabilities coexist.

(L) $G_\nu(\pi/2, 0, \pi/2)$: the scattering of the pair $k_{1\perp} \simeq \pi/2$ and $-k_{2\perp} = 0$, where both the Cooper and Peierls instability are weakened.

Each pair states are illustrated in Fig. 5. Note that, in the actual calculations, π and $\pi/2$ in the arguments of the above coupling constant are replaced as $\pi \rightarrow (30/31)\pi, \pi/2 \rightarrow (16/31)\pi$ due to the finite number of chains.

The flows of the corresponding couplings are shown in Fig. 6. For $E_0(\ell) \gtrsim 4t_\perp$, each couplings are indistinguishable and fully agree with the couplings of the 1D case (the dash-dotted line in Fig. 6). On the other hand, for $E_0(\ell) \lesssim 4t_\perp$, a difference becomes noticeable, indicating the behavior of the interaction is no more 1D, but Q-1D. Thus, we can find the characteristic energy of the crossover as $E_x = 4t_\perp$. This is a clear evidence that the structure of the interaction in Q-1D correlated electrons do exhibit the crossover behavior.

Here a few remarks are in order about the crossover *behavior* and *temperature* appearing in the response functions. In the presence of t_\perp , there is a characteristic temperature for response functions, which are calculated through the RG equations. With decreasing temperature, the effect of t_\perp on the RG equations becomes relevant, suggesting a change of the state from the 1D TLL regime into the 2D regime. Generally, t_\perp in the presence of interaction is renormalized to a reduced value, and the crossover temperature is also renormalized as $T_x^* \sim t_\perp^{1/\phi}$ as obtained from the two-loop RG with the self-energy corrections.^{6,11} Here we distinguish T_x^* (E_x^*) from the bare one. There is no renormalization for T_x ($\sim t_\perp$) at the one-loop level, i.e., no self-energy corrections are included. Nevertheless, a crossover *behavior* does exist in the two-particle quantities at this level of approximation as shown in Fig. 6. The effect of t_\perp on the two-particle correlations such as those contributing to the magnetic susceptibility can be thus obtained even at the one-loop level and the results are expected to carry over to the case where T_x is replaced by T_x^* .

In the Q-1D regime, where $E_0(\ell) \lesssim E_x$, the present N -chain RG shows that the coupling C (P) is reduced (enhanced) compared with the 1D situation. In 1D systems, $(k, -k)$ pairing contributes to both Cooper and Peierls instabilities. In the Q-1D case, however, the Cooper pairing such as in C of Fig. 5 is characterized by bad nesting conditions and contributes weakly to the Peierls instability. The C pairing thus flows to the attractive sector and is attractively relevant. Similarly, for some Peierls pairing such as in P, the contribution to the Cooper instability is weak so that the coupling P flows to the repulsive sector and is repulsively relevant. On the other hand, for Cooper pairs like the C+P, both the Cooper and Peierls instabilities are involved even in the Q-1D regime. In this case, the coupling C+P becomes marginal below E_x . Finally for the pair L, both Cooper and Peierls instabilities are weakened so that coupling L is hardly renormalized. Note that even for the coupling L or C+P, the couplings

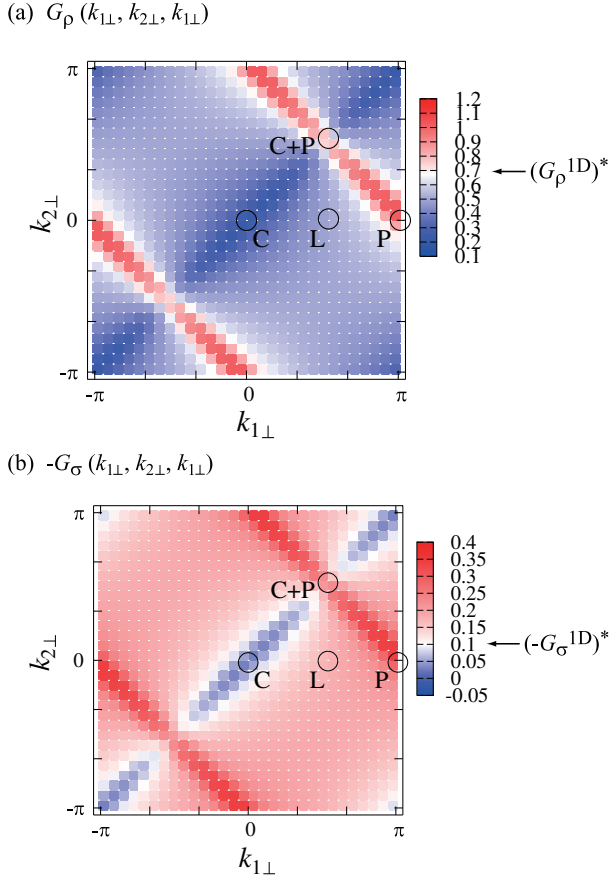


Fig. 7. Renormalized couplings $G_\rho(k_{1\perp}, k_{2\perp}, k_{1\perp})$ (the upper panel) and $-G_\sigma(k_{1\perp}, k_{2\perp}, k_{1\perp})$ (the lower panel) for $U/t = 3.0$, $V_1/t = V_2/t = 0.0$, $t_\perp = 0.01t$ at $T = 10^{-4}t$.

are slightly renormalized in the thermal shell $E_0(\ell) \sim T$ due to the non-logarithmic terms, i.e., the Landau and Cooper+ channels. (See $E_0(\ell)/E_0 \sim 10^{-4}$ in Fig. 6.)

In Fig. 7, we plot the renormalized couplings $G_\nu(k_{1\perp}, k_{2\perp}, k_{1\perp})$ along the plane $k_{1\perp} = k_{3\perp}$ in the parameter-space $(k_{1\perp}, k_{2\perp}, k_{3\perp})$. The function $G_\nu(k_{1\perp}, k_{2\perp}, k_{1\perp})$ is the coupling in the limit of $\mathbf{q} \rightarrow 0$, and thus corresponds to the Landau's interaction function $f(\mathbf{k}_1, \mathbf{k}_2)$, which is the second functional derivative of the energy per unit volume.¹ As we can see from Fig. 7, there are two remarkable structures. One is the valley along $k_{1\perp} = k_{2\perp}$ (the valley C), indicating the Cooper instability of which momenta are \mathbf{k}_1 and $-\mathbf{k}_2$. Another is the ridge along $k_{1\perp} = -k_{2\perp} \pm \pi$ (the ridge P), indicating the Peierls instability reflecting the nesting vector $\mathbf{Q}_0 = (\pm 2k_F, \pm \pi)$. If the system is pure 1D ($t_\perp = 0$), the value of the renormalized couplings are $(G_\rho^{1D})^* \sim 0.7$ and $(-G_\sigma^{1D})^* \sim 0.1$. The valley C is smaller and the ridge P is larger than $(G_\nu^{1D})^*$, indicating that the valley C is more attractive and the ridge P being more repulsive. Moreover, the height of the ridge is not uniform. The cosine-like curve of the valley C suggests the d - or f -wave instability, and the maximum (minimum) of the ridge P suggests the hot (cold) spots of the density-wave instability.⁷ Namely, we can obtain the information of the symmetry of the Cooper pair and the structure of the density-wave fluctuation only from the renormalized

couplings. For the quantitative comparison of each instabilities, we need to calculate the response functions, which are presented in Appendix C

Interestingly, the structure of the present couplings in Q-1D is quite similar to the $f(\mathbf{k}_1, \mathbf{k}_2)$ for the two-dimensional (2D) Hubbard model near half-filling.¹² This suggests that the electronic properties of the Q-1D systems have a lot of similarities with those of 2D systems near half-filling. For example, the Landau parameter F_0^a can also become positive in the Q-1D case, which suggests the possible existence of the spin-dependent zero-sound (zero-spin-sound). This possibility is supported by the decrease of the magnetic susceptibility at low temperatures as shown in the next section. Furthermore, it might be possible that F_1^s becomes negative, which corresponds to the reduction of the Drude weight in the Q-1D case.

The possible fixed points of the couplings in the parameter space $(k_{1\perp}, k_{2\perp}, k_{3\perp})$ are summarized in Fig. 8. The couplings on the C plane $k_{1\perp} = k_{2\perp}$, are attractively relevant due to the Cooper instability. On the P plane where $k_{2\perp} + k_{3\perp} = \pm\pi$, the couplings are repulsively relevant due to the Peierls instability. At the intersection of the C and P planes leading to the C+P line, the couplings are marginal below T_x due to the coexistence of the Cooper and Peierls instabilities. Remaining couplings are hardly renormalized in the Q-1D regime. These conditions for the coupling constants have to be taken into account in order to construct an effective low-energy Hamiltonian in the Q-1D regime.

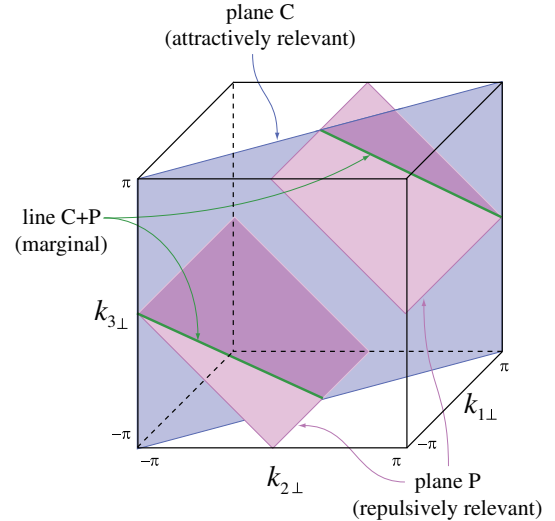


Fig. 8. (Color online) Illustration of the total structure of the fixed points for the couplings G_ρ and G_σ in the parameter space $(k_{1\perp}, k_{2\perp}, k_{3\perp})$. The couplings on the plane C ($k_{1\perp} = k_{2\perp}$) are attractively relevant due to the Cooper instability. The couplings on the plane P ($k_{2\perp} + k_{3\perp} = \pm\pi$) are repulsively relevant due to the Peierls instability. Along the line C+P, the couplings are marginal below T_x due to the interference between Cooper and Peierls instability.

4. Magnetic susceptibility

In this section, we investigate the properties of the magnetic susceptibility. We first briefly review the properties of $\chi(T)$ in the 1D limit¹⁰ and then tackle the main problem of $\chi(T)$ for Q-1D systems by first considering the lowest order perturbation effect of t_\perp with respect to the 1D RPA solution for $(t_\perp/T)^2 \ll 1$, and second by the full one-loop RG treatment where t_\perp is treated non-perturbatively.

4.1 Magnetic susceptibility in 1D

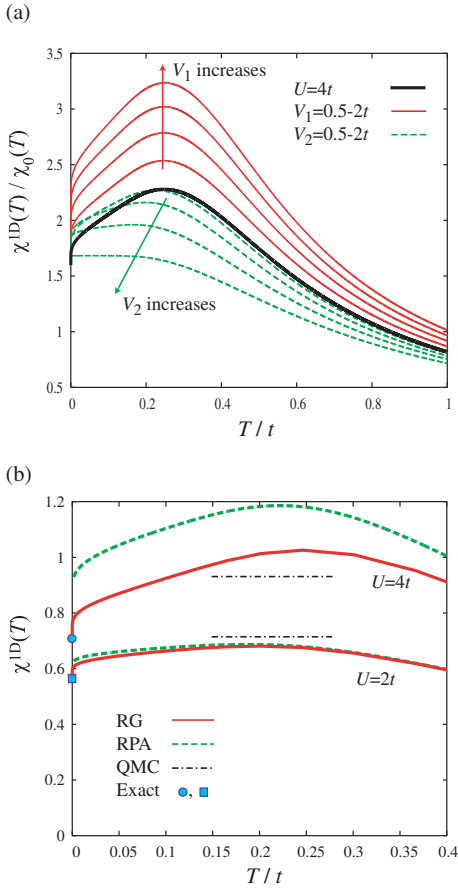


Fig. 9. (Color online) Magnetic susceptibility of 1D, $\chi^{1D}(T)$, as a function of temperature. (a) The black-solid line denotes $\chi^{1D}(T)$ for $U = 4t$, the gray-solid lines denote that for $U = 4t, V_1 = 0.5 \sim 2t$, the gray-dashed lines denote that for $U = 4t, V_2 = 0.5 \sim 2t$. (b) Comparison of $\chi^{1D}(T)$ by RG to the other method. $\chi^{1D}(T)$ by RPA is shown by dashed-lines. The maximum values of $\chi^{1D}(T)$ by QMC locate around the dash-dotted-lines.¹³ The exact solution at $T = 0$ are indicated by the square and circle.

We plot the 1D magnetic susceptibility χ^{1D} in Fig. 9 (a) for $(U, V_1, V_2) = (4t, 0, 0)$ (thick solid-line), $(4t, 0.5 \sim 2t, 0)$ (thin solid-lines), $(4t, 0, 0.5 \sim 2t)$ (thin dashed-lines). (The results coincide with those of Ref. 10, or those of the following section in the limit $t_\perp = 0$.) For the Hubbard model ($U > 0, V_1 = V_2 = 0$), $\chi^{1D}(T)$ is proportional to $1/T$ at high temperatures, has a maximum around $T \sim 0.2t$, and then decreases towards the zero temperature value $\chi^{1D}(0) = (2/\pi v_F)[1 - U/(2\pi v_F)]^{-1}$

with an infinite slope. When V_1 increases, $\chi^{1D}(T)$ is enhanced but the temperature profile remains essentially the same; the influence of V_1 being similar to the one of U . When V_2 increases, however, $\chi^{1D}(T)$ decreases and becomes flat at low temperature, that is $d\chi^{1D}/dT|_{T \rightarrow 0} = 0$ for $U = 2V_2$ (i.e., $g_\sigma = 0$).

In Fig. 9 (b), we compare the temperature profiles of $\chi^{1D}(T)$ for different approaches. The results of the RG are shown by the solid lines and the 1D (renormalized) RPA form for $\chi^{1D}(T)$,

$$\chi_{\text{RPA}}^{1D}(T) = \frac{2}{\pi v_F} \frac{\chi_0(T)}{1 + [G_\sigma(T) - G_{4\perp}(T)]\chi_0(T)/2}, \quad (57)$$

are given by the dashed lines. Here $\chi_0(T) = \tanh(E_0/4T)$ is the bare magnetic susceptibility per branch $p = \pm$ normalized by πv_F . $G_\sigma(T)$ denotes the renormalized coupling at T , which is given by $G_\sigma(T) = G_\sigma/[1 + G_\sigma \ln(2T/E_0)]$, and $G_{4\perp} = (G_{4\rho} - G_{4\sigma})/2$. We can see that eq. (57) includes the fluctuation *beyond* the ordinary RPA, where $G_\sigma(T) = G_\sigma$ is independent of temperature¹³. The maximum values calculated by the quantum Monte Carlo (QMC) technique¹³ (for which low temperatures cannot be reached due to sign problem) are indicated by the dash-dotted lines. The exact solutions at $T = 0$ are shown by the square and the circle for $U = 2t$ and $4t$, respectively.^{13,14}

For $U = 2t$, $\chi^{1D}(T)$ of the RG and renormalized RPA results, eq. (57), quantitatively agrees with that of the exact solution and QMC. However, for $U = 4t$, $\chi_{\text{RPA}}^{1D}(T)$ is sizably larger than the QMC, suggesting that RPA result overestimates the effect of spin correlations. This overestimation is not found in the full one-loop RG result, and $\chi^{1D}(T)$ remains close to that of QMC. This improvement is due to non-logarithmic terms, which becomes effective at high temperatures, and also comes from the mode-mode coupling terms.

Summarizing, the RG prediction for $\chi^{1D}(T)$ agrees well with the exact solution at $T = 0$ even for large U . It also agrees reasonably well with the QMC results at high temperatures, though it only slightly departs from QMC at large U . Therefore the present RG technique yields the most reliable results for the uniform susceptibility in the case of the 1D extended Hubbard model for the wide temperature region $0 \leq T \lesssim t$.

4.2 RPA approach with the perturbation of t_\perp

First we see the variation of the couplings G_ν on the basis of the perturbation of t_\perp . We adopt the 1D Kadanoff-Wilson RG of Ref. 10, as a non-perturbative part. The functions $I_{C,P,L,C+}$ can be expanded in t_\perp (or A_μ) as

$$I_{C,P} \simeq \tanh\left(\frac{E_0(\ell)}{4T}\right) - f(E_0(\ell)/4T) \left(\frac{A_{C,P}}{2T}\right)^2, \quad (58)$$

$$I_{L,C+} \simeq \frac{E_0(\ell)}{4T} \cosh^{-2}\left(\frac{E_0(\ell)}{4T}\right) - g(E_0(\ell)/4T) \left(\frac{A_{L,C+}}{2T}\right)^2, \quad (59)$$

where

$$f(x) \equiv \frac{1}{4x} \left[1 + \left(2x - \frac{1}{x} \right) \tanh x - \tanh^2 x - 2x \tanh^3 x \right], \quad (60)$$

$$g(x) \equiv \frac{x}{3} \frac{2 - \cosh(2x)}{\cosh^4 x}. \quad (61)$$

(Here, we omit the (q, q_\perp, k_\perp) dependence of I_μ and A_μ .) The flow equation (52) for $\mathbf{q} \rightarrow 0$, which is relevant for the magnetic susceptibility, can be rewritten as follows.

$$\overline{G}_\rho(T) = G_\rho^{\text{1D}}(T), \quad (62)$$

$$\overline{G}_\sigma(T) = G_\sigma^{\text{1D}}(T) - 2G_\sigma^2 \bar{f}(T) \left(\frac{t_\perp}{T} \right)^2, \quad (63)$$

$$\overline{G}_{4\rho}(T) = G_{4\rho}^{\text{1D}}(T) + \frac{1}{2}(G_{4\rho}^2 + G_{4\sigma}^2) \bar{g}(T) \left(\frac{t_\perp}{T} \right)^2, \quad (64)$$

$$\overline{G}_{4\sigma}(T) = G_{4\sigma}^{\text{1D}}(T) + G_{4\rho} G_{4\sigma} \bar{g}(T) \left(\frac{t_\perp}{T} \right)^2, \quad (65)$$

and for $G_{4\perp} \equiv (G_{4\rho} - G_{4\sigma})/2$,

$$\overline{G}_{4\perp}(T) = G_{4\perp}^{\text{1D}}(T) + G_{4\perp}^2 \bar{g}(T) \left(\frac{t_\perp}{T} \right)^2, \quad (66)$$

where

$$\overline{G}_\nu(T) \equiv \frac{1}{N^2} \sum_{k_1, k_2} G_\nu(k_{1\perp}, k_{2\perp}, k_{1\perp}; \ell, T) \Big|_{\ell \rightarrow \infty}, \quad (67)$$

and $\bar{f}(T) \equiv \int d\ell f(E_0(\ell)/4T)$, $\bar{g}(T) \equiv \int d\ell g(E_0(\ell)/4T)$. For $T \rightarrow 0$, $\bar{f}(T) \rightarrow 7\zeta(3)/4\pi^2 \simeq 0.213$, $\bar{g}(T) \rightarrow 0$. The flow equations with full-momenta dependence are derived in Appendix B. Here we use the relation

$$\begin{aligned} \sum_{k_1, k_2} \sum_{k'} \{A_C(q_C, q_{C\perp}, k'_\perp)\}^2 &= \sum_{k_1, k_2} \sum_{k'} \{A_P(Q, Q_\perp, k'_\perp)\}^2 \\ &= \sum_{k_1, k_2} \sum_{k'} \{A_{C+}(q', q'_\perp, k'_\perp)\}^2 \\ &= 8t_\perp^2. \end{aligned} \quad (68)$$

Therefore the enhancement of \overline{G}_ν , aside from G_ρ , is proportional to $(t_\perp/T)^2$.

Next, we estimate the magnetic susceptibility with these \overline{G}_ν 's. By extending the RPA form eq. (57), the magnetic susceptibility in Q-1D lead to be

$$[\chi_{\text{RPA}}(T)]^{-1} = \frac{\pi\nu_F}{2\chi_0(T)} [1 + \{\overline{G}_\sigma(T) - \overline{G}_{4\perp}(T)\} \chi_0(T)/2]. \quad (69)$$

By using eqs. (63) and (66), we can write $\chi_{\text{RPA}}(T)$ at $(t_\perp/T)^2 \ll 1$ in the form

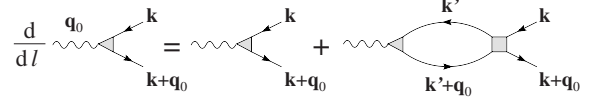
$$[\chi_{\text{RPA}}(T)]^{-1} \simeq (\chi_{\text{RPA}}^{\text{1D}})^{-1} - \frac{\pi\nu_F}{4} [\Delta G_\sigma(T) + \Delta G_{4\perp}(T)], \quad (70)$$

where

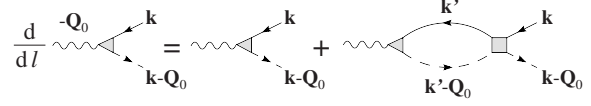
$$\Delta G_\sigma(T) = 2G_\sigma^2 \bar{f}(T) \left(\frac{t_\perp}{T} \right)^2 > 0, \quad (71)$$

$$\Delta G_{4\perp}(T) = G_{4\perp}^2 \bar{g}(T) \left(\frac{t_\perp}{T} \right)^2 > 0. \quad (72)$$

(a) magnetic susceptibility



(b) density wave



(c) superconductivity

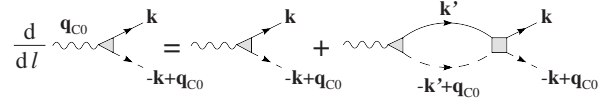


Fig. 10. Diagrams for the renormalization of the pair vertex z_μ at the one-loop level. The triangles and the squares denote the pair vertex and the coupling for (a) the magnetic susceptibility, (b) the density wave, and (c) the superconductivity. The wavy line denotes the corresponding source-fields h_μ .

Consequently, the magnetic susceptibility is enhanced by t_\perp from that of 1D system on the basis of the perturbation theory. Moreover, eq. (70) indicates that a shift from $\chi_{\text{RPA}}^{\text{1D}}$ exists even above $T_x \sim t_\perp$. This suggests that there is no clear feature signaling the crossover from 1D to Q-1D in the temperature dependence of the magnetic susceptibility. This is consistent with the experimental results for the TMTTF and TMTSF salts.⁴

Since this is the perturbation of (t_\perp/T) , one may think that the perturbative form eq. (70) is not valid for $t_\perp/T \sim 1$, namely where the crossover behavior is expected to take place. Even in such case, we can estimate $\chi_{\text{RPA}}(T)$ of eq. (69) from the numerical evaluation of $\overline{G}_\nu(T)$. As is shown later in Figs. 12 and 13, the $\chi_{\text{RPA}}(T)$ so obtained qualitatively agrees with the perturbative form, namely, $\chi_{\text{RPA}}(T)$ is enhanced by t_\perp for the whole temperature region.

4.3 Renormalization group approach

In a path integral approach, the uniform magnetic susceptibility or the response functions can be calculated by adding a set of source fields h_μ to the action. The derivation of response functions is given in Appendix C. In the case of the uniform magnetic susceptibility χ , we introduce the following Zeeman coupling of a source field to the spin density operator:

$$S_\sigma^h[\psi^*, \psi] = \sum_{\tilde{k}, \tilde{q}} [h_p(\tilde{q}) \mathcal{O}_\sigma^*(\tilde{q}, \tilde{k}) + \text{c.c.}]. \quad (73)$$

The one-loop corrections yield

$$\begin{aligned} S_\sigma^h[\psi^*, \psi]_\ell &= \sum_{\{\tilde{k}, \tilde{q}\}^*} h_p(\tilde{q}) z_{\sigma,p}(\tilde{k}, \tilde{k} + \tilde{q}; \ell) [\mathcal{O}_\sigma^*(\tilde{q}, \tilde{k}) + \text{c.c.}] \\ &\quad + \chi_\sigma(\ell) h_p(\tilde{q}) h_p(\tilde{q}). \end{aligned} \quad (74)$$

where $z_{\sigma,p}$ is the pair vertex.

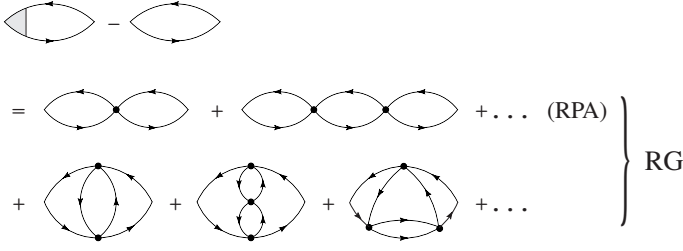


Fig. 11. Diagrams of the magnetic susceptibility contained in the N -chain RG. The dots indicate the bare coupling constants. Diagrams in the second line are considered in the simple RPA.

For the uniform magnetic susceptibility, i.e., $\mathbf{q} \rightarrow \mathbf{q}_0 = 0$, $z_{\sigma,p}$ is expanded in the form¹⁰

$$z_{\sigma,p}(k_{\perp}; \ell + d\ell) = z_{\sigma,p}(k_{\perp}; \ell) + \frac{1}{N} \sum_{k'_{\perp}} z_{\sigma,p}(k'_{\perp}; \ell) G_z(k_{\perp}, k'_{\perp}, k_{\perp}; \ell) \times I_L(q_0, q_{0\perp}, k'_{\perp}; \ell) d\ell, \quad (75)$$

where

$$G_z = -G_{\sigma} + (G_{4\rho} - G_{4\sigma})/2. \quad (76)$$

The corresponding diagram is shown in Fig. 10 (a).

The flow equation for $z_{\sigma,p}$ is obtained as follows:

$$\frac{d}{d\ell} \ln z_{\sigma,p}(k_{\perp}) = \frac{1}{2N} \sum_{k'_{\perp}} G_z(k_{\perp}, k'_{\perp}, k_{\perp}) I_L(q_0, q_{0\perp}, k'_{\perp}). \quad (77)$$

The uniform spin susceptibility in units of $(\pi v_F)^{-1}$ for both branches is given by

$$\chi(T) = \frac{2}{N} \sum_{k_{\perp}} \int_0^{\infty} \frac{d\ell}{\pi v_F} [z_{\sigma,p}(k_{\perp})]^2 I_L(q_0, q_{0\perp}, k_{\perp}). \quad (78)$$

The diagrams which are included in the present method are shown in Fig. 11. It must be noted that mode-mode type of couplings (the third line of Fig. 11) are included in the present calculation. The contribution from these diagrams introduce a qualitative difference for $\chi(T)$ with respect to RPA, as is discussed in the next subsection.

4.4 Susceptibility in the Hubbard limit

The numerical calculation of the magnetic susceptibility is performed by taking $N = 15$, which is large enough to discuss the infinite system in present numerical result. First we calculate the magnetic susceptibility of Q-1D Hubbard model by taking $t_{\perp} > 0, U > 0, V_1 = V_2 = 0$, which is useful to understand the effect of t_{\perp} for weak interaction. Figure 12 shows the magnetic susceptibility as a function of temperature for the small $U (= 1.0t)$ and $t_{\perp} = 0.1 \sim 0.3t$. The behavior of $\chi(T)$ qualitatively agrees with the one found in 1D, where there is a broad peak with a maximum around $T \sim 0.2t$ and a slight drop close to the zero temperature. The effect of t_{\perp} is shown in the inset of Fig. 12, as the ratio of $\chi(T)$ to $\chi^{1D}(T)$. A remarkable enhancement of $\chi(T)$ from $\chi^{1D}(T)$ appears below $T \sim \mathcal{O}(t_{\perp})$. We find that $\chi(T)$ is enhanced by

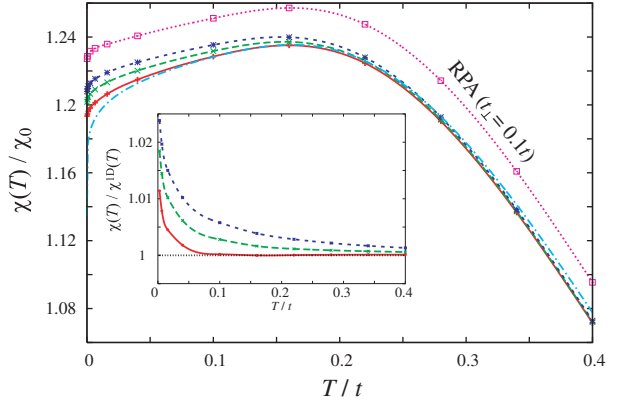


Fig. 12. (Color online) Magnetic susceptibility as a function of the temperature, $\chi(T)$, for $t_{\perp}/t = 0.1 \sim 0.3$ (from bottom to top), $t_{\perp 2} = 0$ with $U = 1.0t, N = 15$. The result by the modified RPA is also plotted for $t_{\perp} = 0.1t$. The inset shows the ratio of $\chi(T)$ in Q-1D to that in 1D, $\chi(T)/\chi^{1D}(T)$.

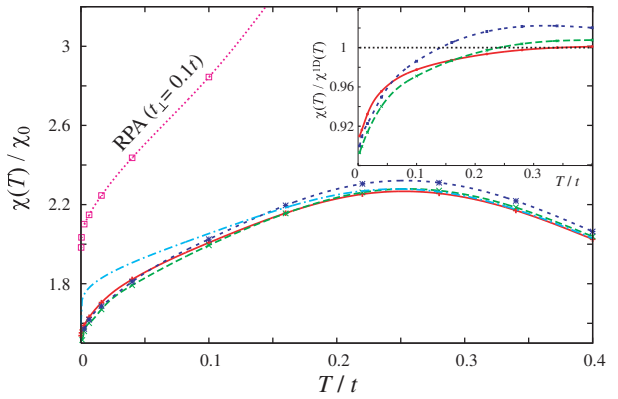


Fig. 13. (Color online) Magnetic susceptibility as a function of the temperature, $\chi(T)$, for $t_{\perp} = 0.1t$ (solid line), $t_{\perp} = 0.2t$ (dashed line) and $t_{\perp} = 0.3t$ (dotted line) with $U = 4.0t, N = 15, t_{\perp 2} = 0$. The dash-dotted line denotes the 1D case. The result by the RPA is also plotted for $t_{\perp} = 0.1t$. The maximum of $\chi_{\text{RPA}}(T)$ for $t_{\perp} = 0.1t$ exceeds $4.0\chi_0$. The inset shows the ratio of $\chi(T)$ in Q-1D to that in 1D, $\chi(T)/\chi^{1D}(T)$.

t_{\perp} as long as U is small. Such a behavior qualitatively agrees with that of the RPA, though the enhancement of $\chi_{\text{RPA}}(T)$ is larger because the RPA overestimates the influence of spin fluctuation.

However, a noticeable feature emerges for large U . Figure 13 shows plots of $\chi(T)$ and $\chi(T)/\chi^{1D}(T)$ for $U = 4t$, and $t_{\perp} = 0.1 \sim 0.3t$. Although the global feature is similar to the 1D case, the qualitative difference appears at low temperatures. Compared with $\chi^{1D}(T)$, $\chi(T)$ is suppressed at low temperatures, whereas $\chi(T) > \chi^{1D}(T)$ is seen at high temperature. Note that this property is similar to that found earlier by Lee *et al.*, who treated only interchain – Coulomb – coupling.⁹

Such an unexpected property definitely differs from the RPA result for susceptibility, which shows an enhancement with respect to the 1D limit over the whole temperature region. The difference in $\chi(T)$ between the

present RG and the RPA@originates mainly from the effect of mode-mode coupling, which represents the result of the quantum interference of each channel, shown in the third line of Fig. 11. The mode-mode coupling term is an higher-order interaction term, so that its effect appears for sizable amplitude of interaction. The RPA overestimates the effect of spin fluctuations especially for the large interaction. Such an overestimation of RPA can be corrected by the mode-mode coupling, as seen from the successful explanation of various experiments on itinerant electron magnetism.¹⁵ The present results for the Q-1D electron systems suggest the important role of the mode-mode coupling (thus the quantum interference of Landau and the other channels) in the N -chain RG. It is worth noticing that for antiferromagnetic spin-fluctuations, their enhancement by the mode-mode coupling also leads to the reduction of $\chi(T)$. This analog situation was discussed for the two-dimensional systems with the nested Fermi surface, where $\chi(T)$ is suppressed by the antiferromagnetic spin-fluctuations due to the mode-mode coupling.¹⁶

This behavior of Q-1D $\chi(T)$ can be understood intuitively as follows. At temperatures higher than t_{\perp} , the 1D fluctuation dominates and suppresses $\chi^{1D}(T)$. However such an effect of 1D fluctuations is weakened by t_{\perp} resulting in the enhancement of $\chi(T)$. On the other hand, at temperatures lower than t_{\perp} , the formation of the SDW (or antiferromagnetic) ordered state is expected due to two-particle interchain couplings. Thus such an effect of the high dimensionality fixing the direction of spin reduces $\chi(T)$ compared to the 1D case. This reduction is specific to spin fluctuations with small momentum transfer $\mathbf{q} = 0$, at variance with spin fluctuations with the large transfer $\mathbf{Q} = (2k_F, \pi)$ (those contributing to the SDW response function) which are enhanced over the whole temperature region by t_{\perp} (see Fig. C.1).

4.5 Susceptibility in the presence of long-range interactions

We now examine the magnetic susceptibility in the presence of the long-range interaction V_i , which takes an important role in the following Q-1D organic conductors. In the TMTTF salts for example, nearest-neighbor repulsion V_1 is expected to be large because of the presence of a charge ordered state.¹⁷ The electronic state of the TMTSF salts, which exhibits the coexistence of SDW and CDW,^{18,19} is explained by taking account the large next-nearest-neighbor repulsion V_2 .^{20,21} The spin-triplet superconducting state in the TMTSF salts²² could be originated from the charge fluctuation, which is enhanced by V_2 .^{21,23-26} In view of these observations for the TMTTF and TMTSF salts, we examine the following two cases. (A) $U > V_1 > 0$, $V_2 = 0$ for the TMTTF salts; (B) $U > V_1 > V_2 > 0$ and $V_2 = U/2$ for the TMTSF salts. We choose the following parameters $(U, V_1, V_2) = (1.6t, 0.7t, 0)$ for (A) and $(U, V_1, V_2) = (0.8t, 0.5t, 0.4t)$ for (B), which give the same power law exponent of the SDW-response function as for $(U, V_1, V_2) = (4.0t, 0, 0)$ in the 1D case.

It should be noticed that the present calculation is performed without the Umklapp scattering, which also

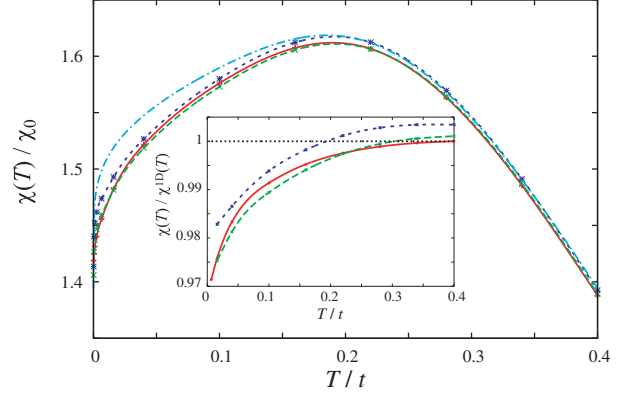


Fig. 14. (Color online) Magnetic susceptibility as a function of the temperature, $\chi(T)$, for $t_{\perp} = 0.1$ (solid line), $t_{\perp} = 0.2$ (dashed line) and $t_{\perp} = 0.3$ (dotted line) with $(U, V_1, V_2) = (1.6t, 0.7t, 0)$, $N = 15$, $t_{\perp 2} = 0$. The dash-dotted line denotes the 1D case. The inset shows the ratio of $\chi(T)$ in Q-1D to that in 1D, $\chi(T)/\chi^{1D}(T)$.

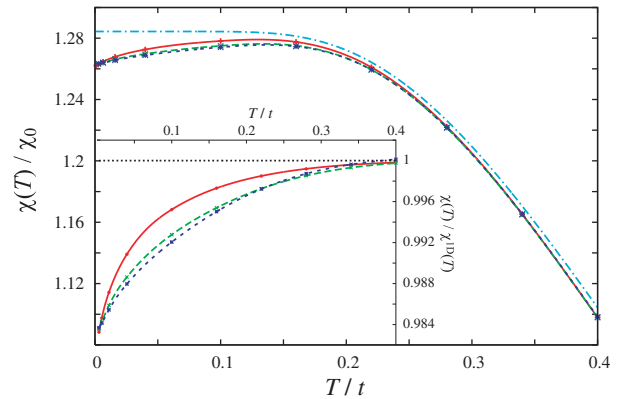


Fig. 15. (Color online) Magnetic susceptibility as a function of the temperature, $\chi(T)$, for $t_{\perp} = 0.1$ (solid line), $t_{\perp} = 0.2$ (dashed line) and $t_{\perp} = 0.3$ (dotted line) with $N = 15$, $t_{\perp 2} = 0$ and $(U, V_1, V_2) = (0.8t, 0.5t, 0.4t)$, where both the SDW and CDW instability are dominant. The dash-dotted line denotes the 1D case. The inset shows the ratio of $\chi(T)$ in Q-1D to that in 1D, $\chi(T)/\chi^{1D}(T)$.

exists at the quarter-filling (i.e., $8k_F$ -Umklapp scattering) and may give rise to a charge ordered state.^{17,27} In 1D case, the charge ordered state does not affect the magnetic properties due to the spin-charge separation. Therefore the present results of $\chi(T)$ without $8k_F$ -Umklapp scattering would be valid at high temperature corresponding to the 1D regime. The effect of Umklapp scattering, which is expected in Q1D regime, could be small even at low temperature, since the magnetic susceptibility of TMTTF salts shows no clear signal around the charge-order transition. Thus the effect of the $8k_F$ -Umklapp scattering is naively expected to be small in the present case in general.^{28,29} However, it still remains as a future problem to clarify the qualitative effect of charge order on the magnetic susceptibility in the Q-1D regime.

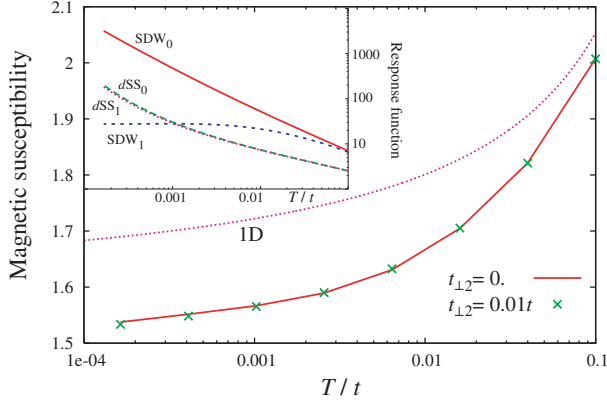


Fig. 16. (Color online) Magnetic susceptibility for $U = 4.0t$, $V_1 = V_2 = 0$, $N = 15$ with $t_{\perp} = 0.1t$, $t_{\perp 2} = 0$ (perfect nesting) and $t_{\perp 2} = 0.01t$ (imperfect nesting). The inset shows the response functions as a function of the temperature. The subscripts i of SDW and dSS indicate the each response function for $t_{\perp 2} = 0$ ($i = 0$) and $t_{\perp 2} = 0.01t$ ($i = 1$).

The temperature dependence of the magnetic susceptibility $\chi(T)$ and its ratio to $\chi^{1D}(T)$ are shown in Fig. 14 for $(U, V_1, V_2) = (1.6t, 0.7t, 0)$ and in Fig. 15 for $(U, V_1, V_2) = (0.8t, 0.5t, 0.4t)$. The SDW instability is the most dominant for the former case, while both the SDW and CDW instabilities become most dominant in the latter case.

As is clear from the plots of the ratio $\chi(T)/\chi^{1D}(T)$, $\chi(T)$ for $V_1, V_2 > 0$ is also reduced from $\chi^{1D}(T)$ at low temperatures. In these cases (especially in the case with $U = 2V_2$), the enhancement of $\chi(T)$ is small, and the relation $\chi(T) < \chi^{1D}(T)$ is seen for the wide range of temperature, i.e., at least for $T < 0.4t$. These features are understood in terms of the coupling $g_{\sigma} (= -U + 2V_2)$. Roughly speaking, the coupling g_{σ} is renormalized to zero as $G_{\sigma}(T) = G_{\sigma}/[1 + G_{\sigma} \ln(2T/E_0)]$, reflecting the effect of the 1D fluctuation. But for $t_{\perp} > 0$, the renormalization is stopped by t_{\perp} as eq. (63), which leads to the enhancement of $\chi(T)$ at high temperatures for the case of the Hubbard model with on-site interaction. On the other hand, for small g_{σ} , the renormalization is small even in the 1D case, i.e., the effect of 1D fluctuation is small. Actually, for $g_{\sigma} = 0$ ($U = 2V_2$), $\chi^{1D}(T)$ is constant at low temperatures as for a normal metal. Thus the enhancement of $\chi(T)$ due to the suppression of 1D fluctuations is less detectable in these situations. These numerical results suggest that reasonable predictions for the pressure dependence of $\chi(T)$ in organic conductors can be made as is discussed in §5.

4.6 Effect of nesting deviations on the susceptibility

So far we have examined the susceptibility for the Q-1D systems with the perfectly-nested Fermi surface, i.e., $t_{\perp 2} = 0$. Since the actual Q-1D conductors exhibits the imperfectly-nested Fermi surface due to the various kinds of interchain hopping, we examine the effect of nesting

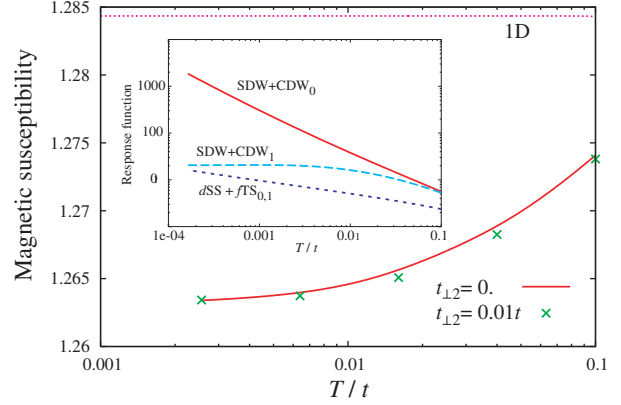


Fig. 17. (Color online) Magnetic susceptibility for $U = 0.8t$, $V_1 = 0.5t$, $V_2 = 0.4t$, $N = 15$ with $t_{\perp} = 0.1t$, $t_{\perp 2} = 0$ (perfect nesting) and $t_{\perp 2} = 0.01t$ (imperfect nesting). The inset shows the response functions as a function of the temperature. The subscripts i of SDW+CDW and $dSS+fTS$ indicate the each response function for $t_{\perp 2} = 0$ ($i = 0$) and $t_{\perp 2} = 0.01t$ ($i = 1$).

deviation by focusing on the simple case of a finite $t_{\perp 2}$. In Fig. 16, the magnetic susceptibility is shown as a function of temperature with $(U, V_1, V_2) = (4.0t, 0, 0)$, where the solid line and the cross denote the susceptibility for the case of the perfect-nesting ($t_{\perp 2} = 0$) and that of the nesting-deviation ($t_{\perp 2} = 0.1t_{\perp}$), respectively. The present case, $t_{\perp 2}/t_{\perp} = 0.1$, is much deviated from the perfect nesting since the quantity $t_{\perp 2}$ treated as the tight-binding approximation in eq. (5) is given by $t_{\perp 2}/t_{\perp} \simeq 0.035$ for quarter-filling. However, $\chi(T)$ for $t_{\perp 2}/t_{\perp} = 0.1$ and $t_{\perp 2} = 0$ are essentially the same, at variance with the response function for SDW, $\chi_s(T)$, shown in the inset of Fig. 16, which levels off below $T \sim t_{\perp 2}$, showing a clear effect of nesting deviations. (For the details of the suppression of the response functions and the nesting property, see Ref. 7,26) In this case d -wave singlet superconductivity becomes dominant at low temperatures. When $t_{\perp 2}$ increases, the ground state moves from a SDW state to a d -wave singlet superconducting states but $\chi(T)$ remains essentially unchanged. Such a difference between χ and χ_s originates from the coupling of the scattering process with the momentum transfer between in- and out-going electrons. The contributions from electron-electron scattering at small momentum transfer $\mathbf{q} \sim 0$ are essential for $\chi(T)$, whereas $\chi_s(T)$ is determined by processes at large momentum

transfer $\mathbf{Q} \sim (2k_F, \pi)$, for which nesting conditions have a strong effect. This fact can be understood easily from the property of the Lindhard response function $\chi_0(\mathbf{q})$, where $\chi_0(q \sim 2k_F)$ is very sensitive to the shape of the Fermi surface.³⁰

For the case with the finite long-range interaction, we plot the numerical results of magnetic susceptibility and some response functions for $U = 0.8t, V_1 = 0.5t, V_2 = 0.4t$ in Fig. 17. For such a case, $V_2 = U/2$, and SDW coexists with CDW in the ground state for $t_{\perp 2} = 0$, whereas d -wave singlet and f -wave triplet superconductivity coexist for $t_{\perp 2} = 0.1t_{\perp}$. The difference in $\chi(T)$ between $t_{\perp 2}/t_{\perp} = 0$ and $t_{\perp 2}/t_{\perp} = 0.1$ is extremely small in spite of this coexistence.

5. Comparison with experiments

In this section, we compare the present results for $\chi(T)$ with those known for the Q-1D organic conductors $(\text{TMTCF})_2X$ ($C = \text{S, Se}; X = \text{PF}_6, \text{Br}$). The latter are summarized as follows.^{4,5} For the compounds $(\text{TMTTF})_2X$ ($X = \text{PF}_6, \text{Br}$), $\chi(T)$ has a maximum at $T \simeq 250\text{-}300\text{K}$, and decreases with an upward curvature as temperature decreases. On the other hand, for $(\text{TMTSF})_2\text{PF}_6$, $\chi(T)$ the maximum of $\chi(T)$ is above room temperature, and the susceptibility decreases approximately linearly with temperature. The temperature variation of $\chi(T)$ is therefore stronger for the TMTTF salts. Since the present results for the Q-1D $\chi(T)$ agree qualitatively with the 1D case, one can discuss its temperature dependence in terms of the results of the 1D system.¹⁰ The stronger temperature dependence of $\chi(T)$ for the TMTTF salts suggests two possibilities: either (i) a large U or (ii) both a large U and V_1 . The weaker temperature dependence of $\chi(T)$ in the TMTSF salts would indicate two possibilities, namely either (i) a small U or (ii) a reasonable combination of U, V_1 and V_2 couplings. The charge ordered state, expected for large V_1 , has been observed in the TMTTF salts.¹⁷ Thus both U and V_1 are expected to be sizable in this family. In the TMTSF salts, it is plausible that U, V_1 and V_2 are large, owing to the SDW and CDW phase coexistence and the possibility of triplet superconductivity for large $U + V_1 + V_2$.^{20,21,25}

Based on the present numerical results shown in §4, we can suggest the following qualitative predictions about the *pressure dependence* of $\chi(T)$ to make the character of these Q-1D conductors more clear. (Here, we assume that the main effect of the pressure is an increase of t_{\perp} .)

- (1) The enhancement of $\chi(T)$ even at low temperature ($T \lesssim 0.1t$) is essentially ascribed to small U .
- (2) The behavior of $\chi(T)$ described by the enhancement at high temperature ($T \gtrsim 0.4t$) and the reduction at low temperature ($T \lesssim 0.1t$) is attributable to the large U ($\sim 4t$) or V_1 .
- (3) The reduction of $\chi(T)$ in the high temperature domain ($T \gtrsim 0.4t$), results from the large V_2 ($\sim U/2$).

However, from the pressure dependence of $\chi(T)$, it is still unclear if these conductors are characterized by interactions with large U or large $U + V_1$. Since the behavior of $\chi(T)$ with $0 < t_{\perp 2} < t_{\perp}$ is almost identical to the case where $t_{\perp 2} = 0$, as discussed in §4.6, the above scenarios

deduced from $t_{\perp 2} = 0$ are also valid when nesting deviations are present and superconductivity is stabilized.

6. Summary and conclusion

In this work, we have extended the Kadanoff-Wilson renormalization group (RG) method to the Q-1D systems. In addition to standard logarithmic terms of the one-loop RG, the present N -chain RG scheme also includes non logarithmic contributions of the Landau and finite momentum Cooper channels. The full (transverse) momentum dependence is retained for all contributions. These are essential to the description of long wavelength spin correlations and enter as key ingredients in the calculation of magnetic susceptibility at finite temperature.

The 1D to Q-1D crossover in the temperature (energy) dependence of the couplings has been obtained. When $T > T_x \sim \mathcal{O}(t_{\perp})$, the flows of the couplings $g_{\nu}(\{k_{\perp}\})$ are essentially independent of the momenta and almost the same as in the 1D case. When $T < T_x$, the flows of $g_{\nu}(\{k_{\perp}\})$ are found to differ and deviations from the 1D case strongly depend on the degrees of quantum interference between various scattering channels that become $\{k_{\perp 1,2,3}\}$ dependent.

The non-perturbative influence of t_{\perp} on the magnetic susceptibility, $\chi(T)$, for Q-1D case has been calculated by the RG technique at the one loop-level and the results compared to different RPA approaches. From the N -chain RG, it is found that for sizable U ($\gtrsim 4t$), the magnetic susceptibility is lower than the 1D case at low temperature ($T \lesssim 0.1t$), but it is enhanced by t_{\perp} at high temperature. This contrasts with the RPA one, $\chi_{\text{RPA}}(T)$, which shows a t_{\perp} -enhancement in the whole temperature region. Such a behavior shows the significant role of t_{\perp} , which depends on temperature. At high temperatures, t_{\perp} suppresses the 1D fluctuation, while it enhances the antiferromagnetic spin-fluctuation at low temperatures. We also note that, for small U (e.g., $U \lesssim t$), both RG and RPA always give the enhancement of $\chi(T)$ by t_{\perp} . The qualitative difference between RPA and RG essentially originates from the effect of mode-mode coupling terms which contribute to the RG flow.

When long-range Coulomb repulsion is added, in particular the next-nearest-neighbor repulsion V_2 , the temperature interval where the susceptibility decreases with respect to the 1D limit extends to higher temperature. With such an effect of t_{\perp} , it may become possible to estimate the magnitude of long-range interactions in Q-1D metals through the pressure dependence of $\chi(T)$.

We have also examined the effect of the nesting deviation on the magnetic susceptibility by introducing the next-nearest-neighbor transverse hopping $t_{\perp 2} > 0$. The response function for CDW and SDW (the $2k_F$ -charge and spin fluctuations) saturates below $T \sim t_{\perp 2}$, while the effect of the nesting deviation is hardly seen for the magnetic susceptibility and the response functions of the superconductivity. Namely, alteration of nesting does not contribute to $\chi(T)$ due to the small-momentum transfer, in contrast to $\chi_{\text{c,s}}(T)$ which are mainly governed by the large-momentum transfer ($\sim 2k_F$) processes.

Acknowledgment

The authors thank T. Giamarchi for valuable discussions. The present work was financially supported by Grants-in-Aid for Scientific Research on Priority Areas of Molecular Conductors (Nos. 15073103 and 15073213) from the Ministry of Education, Culture, Sports, Science and Technology, Japan. Y. F. is supported by JSPS Research Fellowships for Young Scientists.

Appendix A: Contraction of the Landau channel

One of the main improvements of the present N -chain RG from the previous Kadanoff-Wilson RG is that it can take into account the Landau channels, which are non-logarithmic but give relevant contributions at finite temperatures. Here we show how to carry out the contraction of the Landau channels in detail.

The shell average of the quadratic term of the ‘‘Landau’’ action is

$$\begin{aligned} \frac{1}{2} \langle (S_{I,2}^L)^2 \rangle &= 2 \left(\frac{T}{LN} \right)^2 \sum_{p_1 \sim p_4} \sum_{\nu, \nu' = \rho, \sigma, 4\rho, 4\sigma} \\ &\times \sum_{\{\tilde{k}_{1,2}, \tilde{q}\}^*}^{\text{shell}} \sum_{\tilde{k}'} \langle g_\nu(k_{1\perp}, k'_{\perp} - q_{\perp}, k_{1\perp} + q_{\perp}; \ell) \\ &\times \bar{\mathcal{O}}_{\nu, p_1}^*(\tilde{q}, \tilde{k}') \bar{\mathcal{O}}_{\nu', p_2}(\tilde{q}, \tilde{k}') g_{\nu'}(k'_{\perp}, k_{2\perp}, k'_{\perp} - q_{\perp}; \ell) \\ &\times \mathcal{O}_{\nu', p_3}^*(\tilde{q}, \tilde{k}_1) \mathcal{O}_{\nu, p_4}(\tilde{q}, \tilde{k}_2). \end{aligned} \quad (\text{A.1})$$

Here, the definition of $\mathcal{O}_{4\rho}$ and $\mathcal{O}_{4\sigma}$ is the same as \mathcal{O}_ρ and \mathcal{O}_σ , respectively. The corresponding diagrams are shown in Fig. 4 (c). The shell average is given by

$$\begin{aligned} \langle \dots \rangle_{\text{eq. (A.1)}} &= T \sum_{\omega_n} \sum_{\mathbf{k}'}^{\text{shell}} g_\nu(k_{1\perp}, k'_{\perp} - q_{\perp}, k_{1\perp} + q_{\perp}; \ell) \\ &\times g_{\nu'}(k'_{\perp}, k_{2\perp}, k'_{\perp} - q_{\perp}; \ell) \mathfrak{G}_{-p}^0(-\mathbf{k}', \omega_n) \mathfrak{G}_{-p}^0(\mathbf{q} - \mathbf{k}', \omega_n) \\ &= \frac{1}{2\pi v_F} \frac{d\ell}{N} \sum_{k'_{\perp}} g_\nu(k_{1\perp}, k'_{\perp} - q_{\perp}, k_{1\perp} + q_{\perp}; \ell) \\ &\times g_{\nu'}(k'_{\perp}, k_{2\perp}, k'_{\perp} - q_{\perp}; \ell) I_L(q, q_{\perp}, k'_{\perp}; \ell), \end{aligned} \quad (\text{A.2})$$

$$\begin{aligned} I_L(q, q_{\perp}, k'_{\perp}; \ell) &= \frac{E_0(\ell)}{4} \frac{1}{A_L(q, q_{\perp}, k'_{\perp})} \\ &\times \left[\sum_{\lambda=\pm 1} \lambda \tanh \frac{E_0(\ell)/2 + \lambda A_L(q, q_{\perp}, k_{\perp})}{2T} \right], \end{aligned} \quad (\text{A.3})$$

where

$$A_L(q, q_{\perp}, k'_{\perp}) = v_F q + \xi_{\perp}(k'_{\perp}) - \xi_{\perp}(k'_{\perp} - q_{\perp}), \quad (\text{A.4})$$

$$\begin{aligned} v_F q &= v_F(k_3 - k_1) \\ &= \xi_{\perp}(k_{1\perp}) - \xi_{\perp}(k_{1\perp} + q_{\perp}). \end{aligned} \quad (\text{A.5})$$

The function I_L indicates a deviation from the logarithmic divergence, but it does not reach the unity, i.e., the Landau channel is always less logarithmic. Finally, the

Landau contraction yields

$$\begin{aligned} &\frac{1}{2} \langle (S_{I,2}^L)^2 \rangle \\ &= \frac{T}{LN} \sum_{\nu, \nu'} \sum_{\{\tilde{k}_{1,2}, \tilde{q}\}^*} \frac{d\ell}{N} \sum_{k_{\perp}} g_\nu(k_{1\perp}, k'_{\perp} - q_{\perp}, k_{1\perp} + q_{\perp}; \ell) \\ &\times g_{\nu'}(k'_{\perp}, k_{2\perp}, k'_{\perp} - q_{\perp}; \ell) I_L(q, q_{\perp}, k'_{\perp}; \ell) \mathcal{O}_{\nu}^*(\tilde{q}, \tilde{k}_1) \mathcal{O}_{\nu'}(\tilde{q}, \tilde{k}_2). \end{aligned} \quad (\text{A.6})$$

Similarly, the contraction of the Cooper+ channel at the one-loop level is

$$\begin{aligned} \frac{1}{2} \langle (S_{I,2}^{C+})^2 \rangle &= 2 \left(\frac{T}{LN} \right)^2 \\ &\times \sum_{\nu, \nu' = 4||, 4\perp} \sum_{\{\tilde{k}_{1,3}, \tilde{q}'\}^*} \sum_{\tilde{k}'}^{\text{shell}} \langle g_\nu(k_{1\perp}, q'_{\perp} - k_{1\perp}, k'_{\perp}; \ell) \\ &\times \bar{\Delta}_{\nu}^*(\tilde{q}', \tilde{k}') \bar{\Delta}_{\nu'}(\tilde{q}', \tilde{k}') g_{\nu'}(k'_{\perp}, q'_{\perp} - k'_{\perp}, k_{3\perp}; \ell) \\ &\times \Delta_{\nu}^*(\tilde{q}', \tilde{k}_3) \Delta_{\nu'}(\tilde{q}', \tilde{k}_1). \end{aligned} \quad (\text{A.7})$$

The corresponding diagrams are shown in Fig. 4 (d). The shell average is

$$\begin{aligned} \langle \dots \rangle_{\text{eq. (A.7)}} &= T \sum_{\omega_n} \sum_{\mathbf{k}'}^{\text{shell}} g_\nu(k_{1\perp}, q'_{\perp} - k_{1\perp}, k'_{\perp}; \ell) \\ &\times g_{\nu'}(k'_{\perp}, q'_{\perp} - k'_{\perp}, k_{3\perp}; \ell) \mathfrak{G}_p^0(\mathbf{k}', \omega_n) \mathfrak{G}_p^0(\mathbf{q}' - \mathbf{k}', -\omega_n) \\ &= \frac{1}{2\pi v_F} \frac{d\ell}{N} \sum_{k'_{\perp}} g_\nu(k_{1\perp}, q'_{\perp} - k_{1\perp}, k'_{\perp}; \ell) \\ &\times g_{\nu'}(k'_{\perp}, q'_{\perp} - k'_{\perp}, k_{3\perp}; \ell) I_{C+}(q', q'_{\perp}, k'_{\perp}; \ell), \end{aligned} \quad (\text{A.8})$$

$$\begin{aligned} I_{C+}(q', q'_{\perp}, k'_{\perp}; \ell) &= \frac{E_0(\ell)}{4} \frac{1}{A_{C+}(q', q'_{\perp}, k'_{\perp})} \\ &\times \left[\sum_{\lambda=\pm 1} \lambda \tanh \frac{E_0(\ell)/2 + \lambda A_{C+}(q', q'_{\perp}, k'_{\perp})}{2T} \right], \end{aligned} \quad (\text{A.9})$$

where

$$A_{C+}(q', q'_{\perp}, k'_{\perp}) = v_F q' + \xi_{\perp}(k'_{\perp}) + \xi_{\perp}(k'_{\perp} - q_{\perp}), \quad (\text{A.10})$$

$$\begin{aligned} v_F q' &= v_F(k_1 + k_2 - 2k_F) \\ &= -\xi_{\perp}(k_{1\perp}) - \xi_{\perp}(q'_{\perp} - k_{1\perp}). \end{aligned} \quad (\text{A.11})$$

The Cooper+ contraction yields

$$\begin{aligned} &\frac{1}{2} \langle (S_{I,2}^{C+})^2 \rangle \\ &= \frac{T}{LN} \sum_{\nu, \nu'} \sum_{\{\tilde{k}_{1,3}, \tilde{q}'\}^*} \frac{d\ell}{N} \sum_{k_{\perp}} g_\nu(k_{1\perp}, q'_{\perp} - k_{1\perp}, k'_{\perp}; \ell) \\ &\times g_{\nu'}(k'_{\perp}, q'_{\perp} - k'_{\perp}, k_{3\perp}; \ell) I_{C+}(q', q'_{\perp}, k'_{\perp}; \ell) \Delta_{\nu}^*(\tilde{q}', \tilde{k}_3) \Delta_{\nu'}(\tilde{q}', \tilde{k}_1). \end{aligned} \quad (\text{A.12})$$

Appendix B: Perturbation of t_\perp

The contributions of the Cooper and Peierls channels bubbles $I_{C,P}$ and that of Landau and Cooper+ channels, $I_{L,C+}$, are approximated for small t_\perp as

$$I_{C,P} = \frac{E_0(\ell)}{4} \sum_{\lambda=\pm 1} \frac{1}{E_0(\ell) + \lambda A_{C,P}} \times \left\{ \tanh \frac{E_0(\ell)}{4T} + \tanh \frac{E_0(\ell)/2 + \lambda A_{C,P}}{2T} \right\} \simeq \tanh \left(\frac{E_0(\ell)}{4T} \right) - f(E_0(\ell)/4T) \left(\frac{A_{C,P}}{2T} \right)^2,$$

$$I_{L,C+} = \frac{E_0(\ell)}{4} \frac{1}{A_{L,C+}} \left[\sum_{\lambda=\pm 1} \lambda \tanh \frac{E_0(\ell)/2 + \lambda A_{L,C+}}{2T} \right] \simeq \frac{E_0(\ell)}{4T} \cosh^{-2} \left(\frac{E_0(\ell)}{4T} \right) - g(E_0(\ell)/4T) \left(\frac{A_{L,C+}}{2T} \right)^2, \quad (\text{B-1})$$

where

$$f(x) \equiv \frac{1}{4x} \left[1 + \left(2x - \frac{1}{x} \right) \tanh x - \tanh^2 x - 2x \tanh^3 x \right], \quad (\text{B-2})$$

$$g(x) \equiv \frac{x}{3} \frac{2 - \cosh(2x)}{\cosh^4 x}. \quad (\text{B-3})$$

Then, the flow equations (52) can be rewritten in the form:

$$\begin{aligned} \frac{d}{d\ell} G_\rho(k_{1\perp}, k_{2\perp}, k_{3\perp}) &= \frac{d}{d\ell} G_\rho^{1D} \\ &+ \frac{1}{4} (G_\rho^2 + 3G_\sigma^2) \frac{f(E_0(\ell)/4T)}{N} \sum_{k'_\perp} \left\{ \frac{A_C(q_C, q_{C\perp}, k'_\perp)}{2T} \right\}^2 \\ &- \frac{1}{4} (G_\rho^2 + 3G_\sigma^2) \frac{f(E_0(\ell)/4T)}{N} \sum_{k'_\perp} \left\{ \frac{A_P(Q, Q_\perp, k'_\perp)}{2T} \right\}^2 \\ &+ \frac{1}{4} G_\rho (G_{4\rho} - G_{4\sigma}) \frac{g(E_0(\ell)/4T)}{N} \sum_{k'_\perp} \left\{ \frac{A_L(q, q_\perp, k'_\perp)}{2T} \right\}^2 \end{aligned} \quad (\text{B-4})$$

$$\begin{aligned} \frac{d}{d\ell} G_\sigma(k_{1\perp}, k_{2\perp}, k_{3\perp}) &= \frac{d}{d\ell} G_\sigma^{1D} \\ &- \frac{1}{2} G_\sigma (G_\sigma - G_\rho) \frac{f(E_0(\ell)/4T)}{N} \sum_{k'_\perp} \left\{ \frac{A_C(q_C, q_{C\perp}, k'_\perp)}{2T} \right\}^2 \\ &- \frac{1}{2} G_\sigma (G_\sigma + G_\rho) \frac{f(E_0(\ell)/4T)}{N} \sum_{k'_\perp} \left\{ \frac{A_P(Q, Q_\perp, k'_\perp)}{2T} \right\}^2 \\ &- \frac{1}{4} G_\sigma (G_{4\rho} - G_{4\sigma}) \frac{g(E_0(\ell)/4T)}{N} \sum_{k'_\perp} \left\{ \frac{A_L(q, q_\perp, k'_\perp)}{2T} \right\}^2 \end{aligned} \quad (\text{B-5})$$

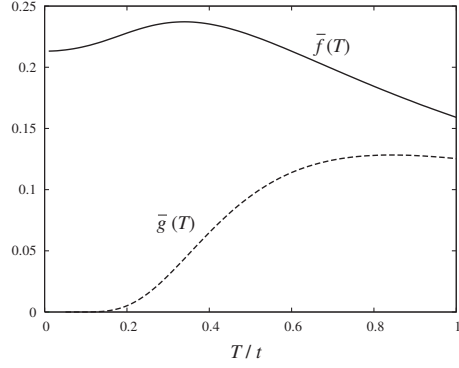


Fig. B-1. Temperature dependences of the functions $\bar{f}(T)$ (solid line) and $\bar{g}(T)$ (dashed line).

$$\begin{aligned} \frac{d}{d\ell} G_{4\rho}(k_{1\perp}, k_{2\perp}, k_{3\perp}) &= \frac{d}{d\ell} G_{4\rho}^{1D} \\ &- \frac{1}{4} \left\{ -2G_\rho^2 + (G_{4\rho} + G_{4\sigma})^2 \right\} \frac{g(E_0(\ell)/4T)}{N} \\ &\times \sum_{k'_\perp} \left\{ \frac{A_L(q, q_\perp, k'_\perp)}{2T} \right\}^2 \\ &+ \frac{1}{4} (G_{4\rho}^2 + G_{4\sigma}^2) \frac{g(E_0(\ell)/4T)}{N} \sum_{k'_\perp} \left\{ \frac{A_{C+}(q', q'_\perp, k'_\perp)}{2T} \right\}^2, \end{aligned} \quad (\text{B-6})$$

$$\begin{aligned} \frac{d}{d\ell} G_{4\sigma}(k_{1\perp}, k_{2\perp}, k_{3\perp}) &= \frac{d}{d\ell} G_{4\sigma}^{1D} \\ &+ \left(\frac{3}{2} G_\sigma^2 - G_{4\rho} G_{4\sigma} \right) \frac{g(E_0(\ell)/4T)}{N} \sum_{k'_\perp} \left\{ \frac{A_L(q, q_\perp, k'_\perp)}{2T} \right\}^2 \\ &+ \frac{1}{2} G_{4\rho} G_{4\sigma} \frac{g(E_0(\ell)/4T)}{N} \sum_{k'_\perp} \left\{ \frac{A_{C+}(q', q'_\perp, k'_\perp)}{2T} \right\}^2. \end{aligned} \quad (\text{B-7})$$

From these equations, the couplings in Q-1D on the basis of a perturbation expansion in t_\perp are obtained. The couplings for $\mathbf{q} = 0$ are shown in §4. It is useful to define the functions $\bar{f}(T) \equiv \int d\ell f(E_0(\ell)/4T)$, $\bar{g}(T) \equiv \int d\ell g(E_0(\ell)/4T)$. The temperature dependences of $\bar{f}(T)$ and $\bar{g}(T)$ are shown in Fig. B-1. In the limit of $T \rightarrow 0$, each function is calculated analytically as $\bar{f}(T) \rightarrow 7\zeta(3)/4\pi^2 \simeq 0.213$, $\bar{g}(T) \rightarrow 0$. As is seen from Fig. B-1, $f(T)$ and $g(T)$ can be treated as constants at low temperatures ($T \lesssim 0.2t$).

Appendix C: Response functions for staggered density-wave and superconductivity

C.1 SDW and CDW responses

We can calculate the SDW and CDW response functions. We add the following S_μ^h terms to the action:

$$S_\mu^h[\psi^*, \psi] = \sum_{\tilde{k}, \tilde{Q}} [h_\mu(\tilde{Q}) \mathcal{O}_\mu^*(\tilde{Q}, \tilde{k}) + \text{c.c.}], \quad (\text{C-1})$$

where $\mu = \text{c, s}$. Here, we concentrate on the response to the source field with the nesting vector $\mathbf{Q}_0 = (2k_F, \pi)$.

This commensurate nesting vector is appropriate for the present Fermi surface, although the incommensurate nesting vector is needed for an arbitrary Fermi surface. The one-loop corrections yield

$$S_{\mu}^h[\psi^*, \psi]_{\ell} = h_{\mu}(\tilde{Q}_0)z_{\mu}(\ell)[\mathcal{O}_{\mu}^*(\tilde{Q}_0, \tilde{k}) + \text{c.c.}] + \chi_{\mu}(\ell)h_{\mu}(\tilde{Q}_0)h_{\mu}(\tilde{Q}_0), \quad (\text{C}\cdot 2)$$

The pair vertex part z_{μ} is expanded in the form

$$z_{\mu}(\ell + d\ell) = z_{\mu}(\ell) - \frac{1}{N} \sum_{k'_{\perp}} z_{\mu}(\ell)G_{\mu}(k_{\perp}, Q_{0\perp} - k'_{\perp}, k'_{\perp}; \ell) \times I_{\text{P}}(Q_0, Q_{0\perp}, k'_{\perp}; \ell)d\ell. \quad (\text{C}\cdot 3)$$

The flow equation for z_{μ}^h is

$$\frac{d}{d\ell} \ln z_{\mu}^h = -\frac{1}{N^2} \sum_{k_{\perp}, k'_{\perp}} G_{\mu}(k_{\perp}, Q_{0\perp} - k'_{\perp}, k'_{\perp})I_{\text{P}}(Q_0, Q_{0\perp}, k'_{\perp}). \quad (\text{C}\cdot 4)$$

In the present paper, we employ the approximation $g_{\mu}(k_{\perp}, Q_{0\perp} - k_{\perp}, k_{\perp}) \simeq g_{\mu}(k_{\perp}, Q_{0\perp} - k'_{\perp}, k'_{\perp})$ and carry out the summation over k'_{\perp} first, since we consider the full-gapped density wave state so that the k'_{\perp} -dependence is irrelevant. The response function in units of $(\pi v_F)^{-1}$ is given by

$$\chi_{\mu}(T) = \frac{2}{\pi v_F} \int_0^{\infty} [z_{\mu}^h]^2 I_{\text{P}}(Q_0, Q_{0\perp}, 0)d\ell. \quad (\text{C}\cdot 5)$$

C.2 Superconductivity response

The quasi-one-dimensionality, i.e., the use of a finite- t_{\perp} , makes anisotropic Cooper pairing possible such as d -wave singlet or f -wave triplet, which cannot be realized in pure 1D systems. Thus we consider not only the full-gapped superconductivity, which have been covered by previous RG calculations, but also for anisotropic superconductivity corresponding to an order parameter with nodes.²¹ We add the $S_{\mu'}$ to the action:

$$S_{\mu'}^h[\psi^*, \psi] = \sum_{\tilde{k}, \tilde{q}_C} [h_{\mu'}(\tilde{q}_C)\Delta_{\mu'}^*(\tilde{q}_C, \tilde{k}) + \text{c.c.}], \quad (\text{C}\cdot 6)$$

where $\mu' = \text{ss}, \text{ts}$. The one-loop corrections yield

$$S_{\mu'}^h[\psi^*, \psi]_{\ell} = \sum_{n, \tilde{q}_C} h_{\mu'}(\tilde{q}_C)z_{\mu'}^{(n)}(\ell)[\Delta_{\mu'}^*(\tilde{q}_C, \tilde{k}) + \text{c.c.}] + \chi_{\mu'}(\ell)h_{\mu'}(\tilde{q}_C)h_{\mu'}(\tilde{q}_C), \quad (\text{C}\cdot 7)$$

At the one-loop level, the pair vertex part is expanded in the form

$$z_{\mu'}^{(n)}(\ell + d\ell) = z_{\mu'}^{(n)}(\ell) - z_{\mu'}^{(n)}(\ell)C_{\mu'}^{(n)}I_{\text{C}}(q_{\text{C}0}, q_{\text{C}0\perp}, 0)d\ell. \quad (\text{C}\cdot 8)$$

The flow equation for $z_{\mu'}^{(n)}$ is

$$\frac{d}{d\ell} \ln z_{\mu'}^{(n)} = -C_{\mu'}^{(n)}I_{\text{C}}(q_{\text{C}0}, q_{\text{C}0\perp}, 0), \quad (\text{C}\cdot 9)$$

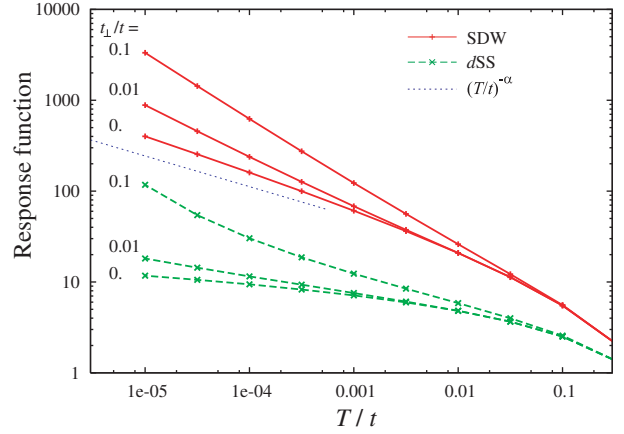


Fig. C.1. Response functions of the SDW (solid lines) and the d -wave singlet superconductivity (dashed lines) for $t_{\perp} = 0, 0.01, 0.1t$ and $U = 3t$.

where $C_{\mu'}^{(n)} (= a_{\mu'}^{(n)}, b_{\mu'}^{(n)})$ is the Fourier coefficients of the coupling $g_{\text{ss}, \text{ts}}$, which are defined in the form

$$G_{\mu'}(k_{\perp}, k_{\perp}, k'_{\perp}; \ell) = a_{\mu'}^{(0)}(\ell) + \sum_{n>0} [a_{\mu'}^{(n)} \cos(nk_{\perp}) \cos(nk'_{\perp}) + b_{\mu'}^{(n)} \sin(nk_{\perp}) \sin(nk'_{\perp})]. \quad (\text{C}\cdot 10)$$

(For the details of the pairing symmetry, see Ref. 21.) The response function in units of $(\pi v_F)^{-1}$ is given by

$$\chi_{\mu'}^{(n)}(T) = \frac{2}{\pi v_F} \int_0^{\infty} [z_{\mu'}^{(n)}]^2 I_{\text{C}}(q_{\text{C}0}, q_{\text{C}0\perp}, 0)d\ell. \quad (\text{C}\cdot 11)$$

The response functions of SDW and d SS for $t_{\perp} = 0, 0.01, 0.1t, U = 3t$ are shown in Fig. C.1. For the 1D case, $\chi_{\text{s}}(T) \sim T^{-\alpha}$ ($\alpha = G_{\rho}/2$), which fully agrees with the well know results of the previous RG.³¹ For $t_{\perp} > 0$, $\chi_{\text{s}}(T)$ is enhanced below T_{x} . The response function for d SS, $\chi_{\text{ss}}^{(d)}$ does not grow for 1D ($t_{\perp} = 0$), because the pairing with nodes is very weak due to the geometric restriction of 1D or due to lack of transverse single coherence. On the other hand, in Q-1D systems, such a pairing becomes possible due to the warping of the Fermi surface. As a result, $\chi_{\text{ss}}^{(d)}(T)$ rapidly grows below T_{x} , though it is less singular than $\chi_{\text{s}}(T)$ in the case of a perfectly nested Fermi surface.

- 1) For example, A. A. Abrikosov, L. P. Gorkov and I. E. Dzyaloshinskii: *Methods of Quantum Field Theory in Statistical Physics*, (Dover, 1975); P. Nozières: *Theory of Interacting Fermi Systems*, (Benjamin, New York, 1964)
- 2) T. Giamarchi: *Quantum Physics in One Dimension*, (Oxford, UK, 2003); Chem. Rev. **104** (2004) 5037.
- 3) J. Moser, J. R. Cooper, D. Jérôme, B. Alavi, S. E. Brown and K. Bechgaard: Phys. Rev. Lett. **84** (2000) 2674.
- 4) M. Dumm, A. Loidl, B. W. Fravel, K. P. Starkey, L. K. Montgomery and M. Dressel: Phys. Rev. B **61** (2000) 511.
- 5) P. Wzietek, F. Creuzet, C. Bourbonnais, D. Jérôme, K. Bechgaard and P. Batail: J. Phys. I **3** (1993) 171.
- 6) C. Bourbonnais, B. Guay and R. Wortis: *Theoretical Methods for Strongly Correlated Electrons*, ed. D. Sénéchal, A. -M. Tremblay and C. Bourbonnais (Springer-Verlag, New York, 2004) p. 77.

- 7) R. Duprat and C. Bourbonnais: Eur. Phys. J. B **21** (2001) 219.
- 8) V. J. Emery, R. Bruinsma and S. Barisic: Phys. Rev. B **48** (1982) 1039.
- 9) P. A. Lee, T. M. Rice and R. A. Klemm: Phys. Rev. B **15** (1977) 2984.
- 10) Y. Fuseya, M. Tsuchiizu, Y. Suzumura and C. Bourbonnais: J. Phys. Soc. Jpn. **74** (2005) 3159.
- 11) J. Kishine and K. Yonemitsu: Int. J. Mod. Phys. B **16** (2002) 711.
- 12) Y. Fuseya, H. Maebashi, S. Yotsuhashi and K. Miyake: J. Phys. Soc. Jpn. **69** (2000) 2158.
- 13) H. Néglise, C. Bourbonnais, H. Touchette, Y. M. Vilk and A.-M. S. Tremblay: Eur. Phys. J. B **12** (1999) 351.
- 14) H. Shiba: Phys. Rev. B **6** (1972) 930.
- 15) T. Moriya: *Spin Fluctuations in Itinerant Electron Magnetism* (Springer-Verlag, Berlin, 1985).
- 16) K. Miyake and O. Narikiyo: J. Phys. Soc. Jpn. **63** (1994) 3821.
- 17) For example, see H. Seo, C. Hotta and H. Fukuyama: Chem. Rev. **104** (2004) 5005.
- 18) J. P. Pouget and S. Ravy: J. Phys. I (Paris) **6** (1996) 1501.
- 19) S. Kagoshima, Y. Saso, M. Maesato, R. Kondo and T. Hasegawa: Solid State Commun. **110** (1999) 479.
- 20) N. Kobayashi, M. Ogata and K. Yonemitsu: J. Phys. Soc. Jpn. **67** (1998) 1098.
- 21) Y. Fuseya and Y. Suzumura: J. Phys. Soc. Jpn. **74** (2005) 1263.
- 22) I. J. Lee, P. M. Chaikin and M. J. Naughton: Phys. Rev. Lett. **78** (1997) 3555; I. J. Lee, S. E. Brown, W. G. Clark, M. J. Strouse, M. J. Naughton, W. Kan and P. M. Chaikin: Phys. Rev. Lett. **88** (2002) 017004.
- 23) K. Kuroki, R. Arita and H. Aoki: Phys. Rev. B **63** (2001) 094509.
- 24) Y. Fuseya, Y. Onishi, H. Kohno and K. Miyake: J. Phys.: Condens. Matter **14** (2002) L655.
- 25) Y. Tanaka and K. Kuroki: Phys. Rev. B **70** (2004) 060502(R).
- 26) J. C. Nickel, R. Duprat, C. Bourbonnais and N. Dupuis: Phys. Rev. Lett. **95** (2005) 247001.
- 27) H. Yoshioka, M. Tsuchiizu and Y. Suzumura: J. Phys. Soc. Jpn. **70** (2001) 762.
- 28) M. Tsuchiizu, H. Yoshioka and Y. Suzumura: J. Phys. Soc. Jpn. **70** (2001) 1460.
- 29) S. Ejima, F. Gebhard and S. Nishimoto: Europhys. Lett. **70** (2005) 492.
- 30) For example, G. Grüner: *Density Waves in Solids*, (Addison-Wesley, 1994)
- 31) J. Solyom: Adv. Phys. **28** (1979) 201.